Design of a Bidirectional Energy Buffer Using a Switched-Capacitor Converter and Supercapacitors for an Auxiliary EIS Converter for Fuel Cell Stacks

by

Behnam Mohammad

B.Sc. (Electrical-Control Engineering), Azad University, 2013

Thesis Submitted in Partial Fulfillment of the
Requirements for the Degree of
Master of Applied Science

in the
School of Mechatronic Systems Engineering
Faculty of Applied Sciences

SIMON FRASER UNIVERSITY
Fall 2020

Declaration of Committee

Name:	**Behnam Mohammad**
Degree:	**Master of Applied Science (Mechatronic Systems Engineering)**
Title:	**Design of a Bidirectional Energy Buffer Using a Switched-Capacitor Converter and Supercapacitors for an Auxiliary EIS Converter for Fuel Cell Stacks**
Committee:	**Chair:** Helen Bailey Lecturer, Mechatronics Systems Engineering
	Jiacheng (Jason) Wang Supervisor Associate Professor, Mechatronics Systems Engineering
	Patrick Palmer Committee Member Professor, Mechatronics Systems Engineering
	Mohammad Narimani Examiner Lecturer, Mechatronics Systems Engineering

Abstract

Fuel cell as an attractive clean energy source has gained a great deal of interest. To increase the durability and reliability of fuel cells, diagnostics systems that can detect degradation and faults inside fuel cell stacks in end applications are highly in need. Electrochemical impedance spectroscopy (EIS), among other methods, is a promising characterizing tool for diagnostics and condition monitoring of fuel cells. It was traditionally only applied to single-cell or short stacks at low-power levels and required special laboratory equipment, but was recently brought to high-power stacks too which was made possible by many technological advancements. This is mainly owing to a growing interest in performing in situ EIS as a non-destructive method without the need for dismantling the stack. Unlike traditional approaches which relied on extra equipment, converter-based EIS provides attractive solutions for this purpose. In this thesis, the design and utilization of a bidirectional energy buffer module composed of a switched-capacitor converter (SCC) and a supercapacitor string for a new auxiliary EIS converter solution is presented. The module is designed towards having a more compact auxiliary converter unit. The design of the proposed energy buffer module is investigated in detail and a guideline is provided considering the application-specific optimal conversion ratio, supercapacitor string capacitance, and the probable limitations imposed by high EIS frequencies on certain situations. In a nutshell, the proposed switched-capacitor converter module (SCCM) consists of a bidirectional high voltage-gain SCC connected with supercapacitor string helps with the compactness and miniaturization of the entire auxiliary EIS converter and eliminating the potential problems of electrolytic capacitors such as bulkiness and limited lifetime due to the impact of ripples. The SCCM energy buffer with a high voltage gain offers a high buffering ratio for utilizing supercapacitors as the energy storage device.

Keywords: Energy Buffer, Converter-based EIS, AC Perturbation, Switched-Capacitor Converter, Energy Buffer with High Buffering Ratio

Acknowledgments

I would like to greatly thank my senior supervisor Dr. Wang for his enormous help, guidance, and kindness, coming back to school was a great opportunity and being his student was a privilege and a great chance to advance my education. Also, I would like to express my appreciation to Dr. Palmer for his great guidance and help throughout my schooling and accomplishing this work.

Thank you very much to all my friends in PEEAL lab, Jiabin Shen, Matt Greig and Jiajie Zang for their friendship and guidance during my master's and hopefully many more years to come. Thanks to my office mates Zayed, Vahideh, Charles and Wayne Lye for their friendship and sharing many good moments together.

I want to sincerely thank my family Soraya, Ali, Bahram, and Samira for their emotional and financial supports especially my dad Hossein who means the world to me.

Table of Contents

List of Tables

List of Figures

List of Acronyms

DER	Distributed Energy Resources
DRC	Design Rules Check
EMS	Energy Management System
ERC	Electrical Rules Checking
ESR	Equivalent-Series Resistance
FC	Fuel Cell
FCS	Fuel Cell Stack
ICE	Internal Combustion Engine
MCU	Microcontroller Unit
PCC	Power Conditioning Converter
PEM	Proton Electrolyte Membrane
RUL	Remaining Useful Life
SC	Supercapacitor
SCC	Switched-Capacitor Converter
SCCM	Switched-Capacitor Converter Module
TDPR	Total Device Power Rating

Chapter 1.

Introduction

The fuel cell (FC) as a clean energy source has attracted significant interest over the past several decades, but its development and commercialization are still hindered due to a few major shortcomings such as high cost, limited lifetime, and reliability. In addition to the evolvement of FCs and its systems, development of tools capable of characterizing FC stacks and monitoring the internal status is important since they help with studies of degradation and faults and lead to improved power and energy management in end applications. Electrochemical impedance spectroscopy (EIS) is a promising tool for the characterization of FCs. It was traditionally only applied to single-cell or short stacks at low-power levels but recently owing to the enormous ongoing research, is brought up to high-power levels due to growing interest in performing in situ EIS as a non-destructive method without the need for dismantling the FC stack. In this thesis, an auxiliary converter dedicated for EIS perturbation generation is introduced for use with high-power FC stacks. In order for the EIS auxiliary converter to be able to provide the EIS perturbation and absorb the resulted ac signals, an energy buffer module utilizing a high conversion ratio bidirectional SCC connected to a string of supercapacitors at the low side of the converter is proposed. This energy buffer solution, named as a switched-capacitor converter module (SCCM), is an alternative solution for other instantaneous types of energy storage technologies such as electrolytic capacitors. As a result of the much lower voltage ratings of commercially available supercapacitors compared to electrolytic capacitors, a high conversion ratio is needed and is accomplished via an SCC employed as an interface. The bidirectional SCC with high voltage gain enables the proposed energy buffer system to provide the necessary high buffering ratio for the supercapacitor string.

1.1. Introduction to PEM Fuel Cell Technology

As a clean source of energy and an attractive alternative to traditional energy sources such as fossil fuel and steam engines, FCs are used in stationary applications such as grid-connected and back-up power supplies [1] as well as different transportation systems such as heavy-duty vehicles [2],[3], electric aircrafts, and drones [4]. FCs are also used as range-extenders for battery-powered vehicles [5]. In general, FCs generate electricity by combining hydrogen and oxygen supplied to different sides of a membrane with the only by-product of water. It is therefore considered as a promising clean energy source [6]. During this electrochemical energy conversion, undesirable conditions such as flooding, dehydration (drying), and oxidant starvation contribute to FC degradation and are the main causes for the limited life of FCs and their high maintenance cost [7].

One of the well-known and promising types of FC technology is proton exchange membrane (PEM) that has many advantages such as high-power density, fast start-up, discontinuous operation, and relatively low operating temperature [8] which makes it a great candidate for the abovementioned applications over other existing FC technologies [7]. Although the FC is one of the oldest electrical energy-conversion technologies, its development had been lagging compared to internal combustion engine (ICE) and steam engines due to the relatively high cost, materials problems, and certain inadequacies in the operation of electrochemical devices such as the electrodes and membranes, stated in [4] and [9].

Having reliable diagnosis systems can solve a big portion of material problems and significantly increase the durability of FC stack by enabling the energy management system (EMS) to identify the current internal state of FC stacks. Conditions such as flooding of anode and cathode, drying and dehydration of membrane, and cathode and anode corrosion are undesired conditions as their occurrence can potentially cause permanent damages to the FC.

Therefore, to improve the durability of PEM FC stacks, having the ability to identify the abovementioned undesirable conditions inside the FC stack is considered to be crucial, leading to an emphasis on the need for a reliable diagnosis system.

1.2. Fuel Cell Diagnostics Tools and Techniques

Despite the importance and need of continuous advancement for developing more durable FCs, one of the ways to avoid FC stacks from premature aging with the ultimate goal of prolonging their life expectancy and increase durability is by implementing a good EMS equipped with a diagnostic system. There are several techniques developed to extract the internal state of an FC. Methods such as voltage sweeping (VS), voltage cycling (VC) [10], total harmonic distortion analysis (THDA) [11], cell voltage monitoring (CVM) [12], and EIS have all been used to provide FC internal information and help with its condition monitoring, operation evaluation, and regular and preventative maintenance scheduling [13]. Among all, the EIS method measures the internal impedance of an FC revealing rich information of its internal state and is known to be a valuable tool for FC stack characterization [14], [15] and [16]. Typically, EIS is only applied to single cells or short stacks at low power settings. There has been growing interest lately to adapt this tool for use with high-power FC stacks since applying it directly at the stack level allows characterizing the stacks without the need of dismantling the entire system for laboratory testing. Like many other electrochemical components such as lithium-ion batteries and supercapacitors (SC), the measured internal impedance is an indicator of their degradation, state-of-health (SoH) [7] and [17], or remaining useful life (RUL) [18]. Therefore, the data obtained through EIS methods can drastically contribute to the improvement of the durability of FCs.

1.3. Fuel Cell Electrochemical Impedance Spectroscopy

In a nutshell, EIS is a method for measuring the internal impedance of the FC stacks. This method has been used for many similar electrochemical energy storage devices such as lithium ion batteries and supercapacitors. As the electrochemical cell ages, naturally, its internal impedance changes. For FC, certain conditions such as flooding, drying, oxidant dehydration also result in unexpected changes in the internal impedance.

As a non-destructive technique, EIS is a promising tool for characterizing fuel cells. Considering the FC as a black box, its terminals are where the generated perturbation can

be injected into the FC stack. There are different methods for performing EIS on FC stacks such as using linear power amplifiers, half bridge, or a full bridge to generate the ac perturbation signals. By generating and injecting different frequencies for ac excitation signals into the FC stack and measuring their response, different impedance are measured. As the FC stack cycles, the impedance measured grows naturally but in cases, where flooding, drying, and oxidant starvation occurs, as a result of a change in impedance, the extracted data can be interpreted towards identifying the current internal state and estimation of state-of-health (SoH) of the FC stack. A typical impedance spectrum of a fuel cell is depicted in Figure 1-1 [13].

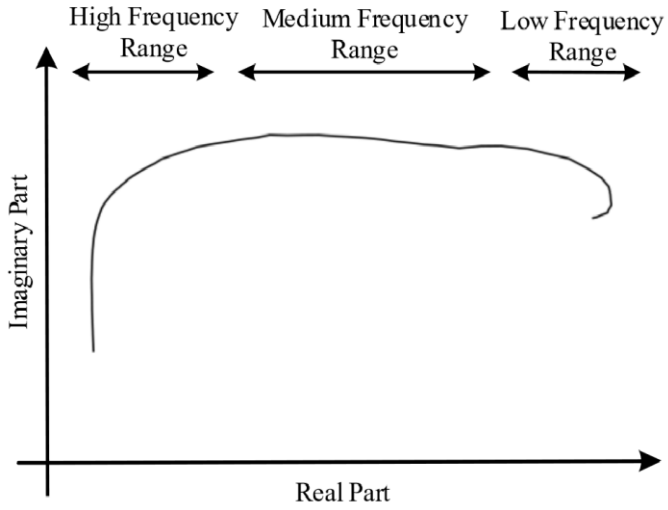

Figure 1-1 Typical Impedance Spectrum of a fuel cell stack.

1.4. Converter-based EIS

Traditionally, performing EIS required special equipment and was mostly done in offline testing settings. Offline EIS equipment tends to be expensive and require the FC stack to be disconnected from the system. Offline mode refers to when FC stack is disconnected, and online method refers to a technique that the FC stack is still able to independently operate while EIS testing is being performed. However, adopting offline EIS for FC stacks while the system is running was a challenging task. The goal of performing EIS is to be able to extract meaningful information from the FC stack while the FC system is operating, without halting the process and availability. In the traditional way

of performing EIS there is a need for disassembling the FC stack. One of the tools used for performing fuel cell EIS diagnosis is by utilizing power amplifiers which are usually used for single or short stacks. However, these are limited by their relatively low power rating. Although there is some ongoing research on voltage reduction of the FC stack [19], more improvements are still required for this method. On the other hand, switching converter-based EIS is more attractive in terms of the capability to handle the large power rating at stack levels as compared to linear amplifiers. One of the challenges with performing online or *in situ* EIS is how to effectively produce an excitation signal at different frequencies and measure the response. The challenges are mainly related to the presence of other voltage and current components resulted from the DC operating point of the FC stack. The issues of properly producing a wide frequency range of ac excitation with the main power conditioning converter (PCC) are addressed in [20]. Alternatively, the interesting concept of decoupling the EIS signal generating converter from the main power unit was introduced in [15] and [21]. Here, an auxiliary EIS converter, e.g., a half bridge, which can be also replaced by a full bridge or other topologies, is decoupled from the main PCC and as such offers a more flexible and potentially compact solution for generating the ac perturbations.

1.5. Auxiliary EIS Converter

Although having a dedicated converter to generate EIS perturbations may raise the question of space constraint of FC-powered vehicles, this study is targeting heavy-duty vehicles that relatively have more powertrain room to house this auxiliary EIS converter. Therefore, the beneficial role of this converter outweighs the space constrain of FC-powered vehicles. Moreover, supercapacitors have much higher energy density [22] and [23], therefore, it is a more compact energy storage technology compared with electrolytic capacitors and other counterparts. Thus, utilizing a compact bidirectional interface such as an SCC (as explained before) contributes to a more compact solution.

The benefits of having an auxiliary EIS converter for FC technology can be listed as 1) As a plug and play module that provides great flexibility, 2) Decoupling the main power conditioning converter (PCC) from perturbation generating device, 3) The auxiliary EIS converter only needs to be sized to process the ac perturbations and does not need to handle

the main power (referring to the DC operating point) from the FCS, and thus, resulting in a compact module.

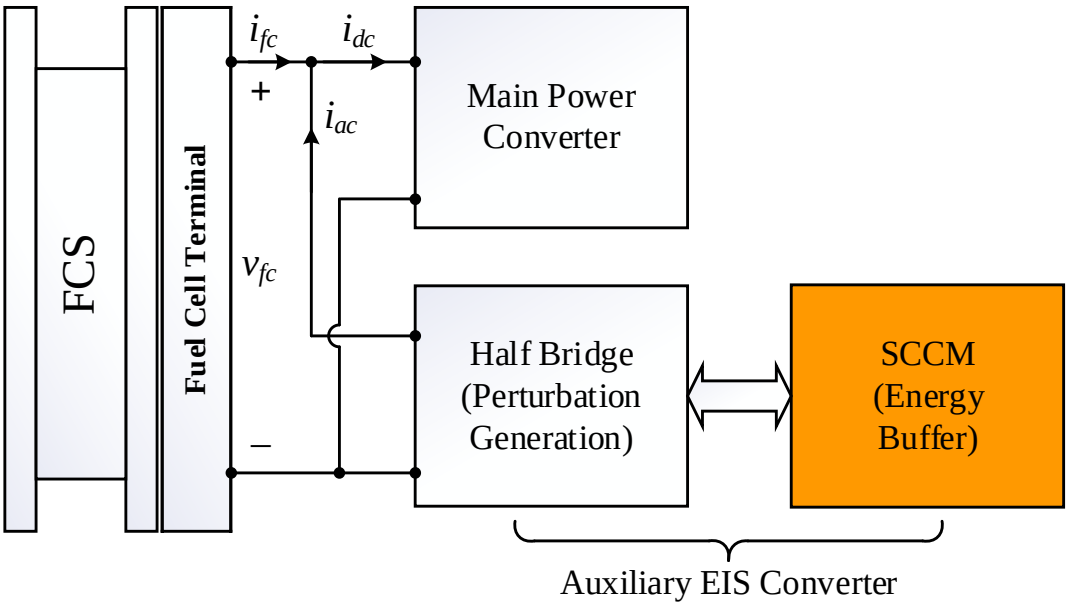

Figure 1-2 Overview of the Auxiliary EIS system with SCCM

As shown in Figure 1-2, the proposed auxiliary EIS converter is composed of two parts. The first part is the controlled half-bridge shown on the left side which is responsible for generating EIS signals. The required ac perturbations, typically from sub-hertz to a couple of kHz for FCS EIS, are modulated through the converter following its current reference. The second part is the uncontrolled SCCM that is operated in an open-loop mode with a complimentary pair of PWM signals. The proposed module should be able to provide voltage support for the half-bridge when generating ac perturbation signals, requiring the SCCM to operate in boost mode operation (boost the voltage of the supercapacitor string to required level). It should also be able to absorb the oscillations from EIS excitations when the SCCM is operating in the buck mode (stepping down the half-bridge voltage to the level which is within the allowable rated voltage for the supercapacitor string). It should be mentioned that the controlled half-bridge can be replaced with other choices such as a full bridge converter. The focus of the thesis is placed on the design of the bidirectional SCCM.

As previously mentioned, one of the important advantages of an auxiliary EIS converter is its decoupling state from the main power converter; thus, it only needs to be sized to process the EIS perturbations injected into the FC cells/stacks. Normally, the ac current perturbation is set to 10% of its dc operating point [24] and is expressed as:

$$i_{ac} = 0.1 I_{fc} \sin(\omega t) \tag{1.1}$$

where I_{fc} is the magnitude of the fuel cell output current and ω is the angular frequency of the ac perturbation. A simplified model of an FCS is shown in Figure 1-3 using the Randle's equivalent circuit. After applying the EIS signals, the output voltage to be processed by the EIS auxiliary converter is composed of both dc and ac components. The ac component is denoted as P_{ripple} due to the existence of the ac signal and dc bias. ($Z_m = R_1 + \frac{R_2}{1+R_2 j\omega C}$).

$$v_{fc} = V_{OC} - Z_m(I_{fc} + i_{ac}) \tag{1.2}$$

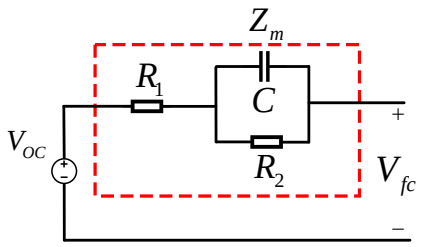

Figure 1-3 Fuel cell stack model with Randle's circuit

After applying the ac perturbation signals on top of the DC operating point of the FC stack formulated in (1.2), the instantaneous output power of the fuel cell is written as:

$$P_{fc} = (V_{OC} - V_{Zm})(I_{fc} + i_{ac}) \tag{1.3}$$

Substituting (1.1) into (1.3) we have:

$$P_{fc} = I_{fc}\left(V_{OC} - (R_1 + \mathrm{R}_2)I_{fc}\right) - 0.1 Z_m I_{fc}^2 \sin(\omega t) + 0.1\left(V_{OC} - (R_1 + \mathrm{R}_2)I_{fc}\right)I_{fc} \sin(\omega t) - 0.01 Z_m I_{fc}^2 \sin^2(\omega t) \tag{1.4}$$

After eliminating the dc and double frequency components, the remaining ac ripple part of P_{fc}, P_{ripple} is the exchanged power during the charging and discharging of the SCCM module. As mentioned at the beginning of this section, the EIS auxiliary converter needs to be sized and capable of withstanding P_{ripple}.

1.6. Energy Buffer for the Auxiliary EIS Converter

The energy buffer is an important part of the auxiliary converter and there are different approaches of its implementation. Energy buffers are widely used in various applications. An energy buffer is proposed in [25] as a replacement for the decoupling electrolytic capacitor, adding durability to the ac-dc converter. A bank of ceramic capacitors is used as energy storage devices interfacing with an SCC with a 1:2 buffering ratio. A general explanation and techniques for developing a bidirectional inductor-based dc-dc converter to interface supercapacitors were examined in [26] which due to the perception of the inability of SCC in handling high power applications [27], SCCs were not examined. The proposed energy buffer SCCM utilizes a bidirectional high voltage gain SCC [28] to interface with a supercapacitor string due to the low voltage rating of supercapacitor cells (typically 2.5V~3V [29]). In Figure 1-4 a depiction of energy buffering is provided for better visualization.

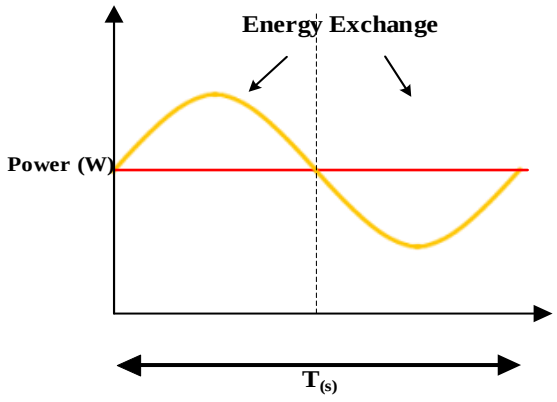

Figure 1-4 Energy buffering depiction

1.6.1. Switched-Capacitor Converter

To revisit some of the definitions used in this work, conversion ratio is defined as the ratio of output to the input voltage $M(D) = \frac{V_{OUT}}{V_{IN}}$. In this application, despite the historical belief that SCCs are suitable for low power rating applications due to technology limitations [27], it is perceived that the switched-capacitor converter (SCC) has possible advantages and uniqueness over other dc-dc converters for certain high-power applications. An SCC with 1:3 conversion ratio is depicted in Figure 1-5. The capability of its performance for higher power rating applications was investigated in [28]. Also, recently, SCCs are subject to much research and investigation for miniaturization and portable devices. A comprehensive comparative assessment between inductor-based and inductor-less dc-dc converters was presented in [30] which elaborates on the features of SCCs in terms of compactness, power density, cost, and scalability.

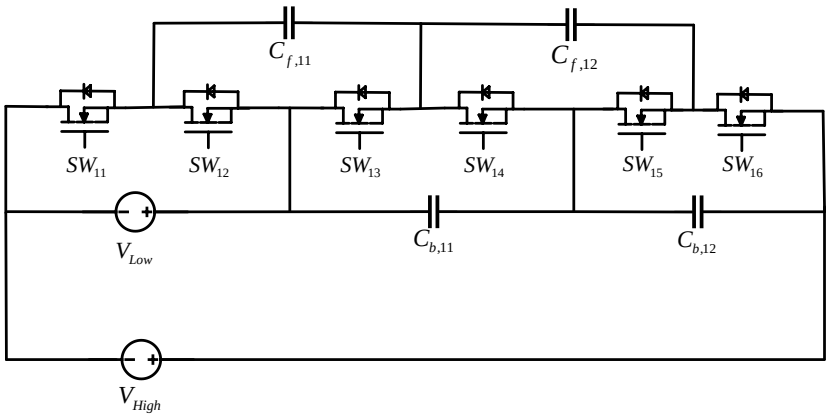

Figure 1-5 SCC diagram with 1:3 conversion ratio

1.6.2. Working Principle and the Role of Energy Buffer Module

As explained previously, the EIS auxiliary converter needs an instantaneous energy storage device to provide the required energy to generate the ac signal and be able to absorb the resulted signals from the ac excitations. One solution for the instantaneous energy storage device is an electrolytic capacitor which is available in a wide range of voltage ratings and capacitances [31]. However, their relatively low energy density increases the size of the entire auxiliary EIS converter, not to mention the dramatic cost increase based

on the rated voltage and the impact of ripples on the lifetime of electrolytic capacitors. Another instantaneous device for storing energy is a supercapacitor with a relatively much higher energy density, however, due to the relatively low voltage rating for commercially available supercapacitors, to reach the minimum required voltage defined by the EIS converter, a bidirectional converter is required. Therefore, as a direct replacement for the electrolytic capacitor , this energy buffer module is proposed.

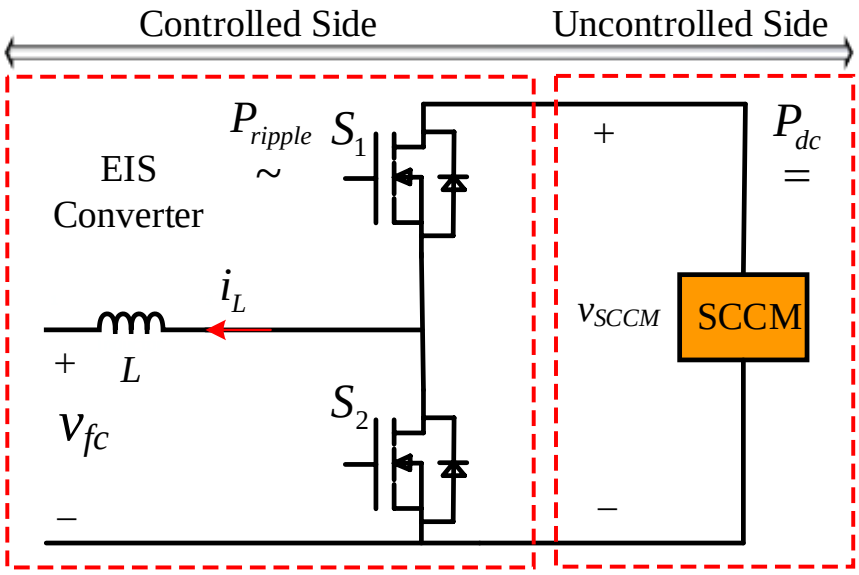

Figure 1-6 Auxiliary EIS converter setting

The energy buffer module shown in Figure 1-6 consists of a high gain bidirectional SCC interfacing with a string of supercapacitors. The supercapacitor string serves as the required energy storage device while the SCC is functioning as an interface between the auxiliary EIS converter and the supercapacitor string. The ac perturbation signals are injected into the FC stack and the resulting signals are measured for analysis revealing the internal state of the FC stack. As can be seen in Figure 1-2 the required energy for generating EIS signals is provided by the supercapacitors string via the SCC and during the buck operation, the resulted signals from the FC stack through the EIS converter are absorbed by the supercapacitors string.

To have a more detailed look at the Figure 1-6, one side is marked as controlled where the half-bridge is assigned for EIS perturbation generation and the uncontrolled side is a passive energy buffer. The control principle of the SCC is based on charge sharing (charge redistribution) through the capacitors' network. The direction of charge is orchestrated via a complementary pair of PWM signals generated by a signals generator, microcontroller (MCU), or a timer IC. The auxiliary EIS converter is a buck converter which can boost up the voltage when current is going the opposite direction, meeting the working requirement for the half-bridge which is $V_{SCCM} > V_{fc}$. The energy exchange is depicted in Figure 1-7 as an explanatory graph to demonstrate the functionality of the proposed energy buffer.

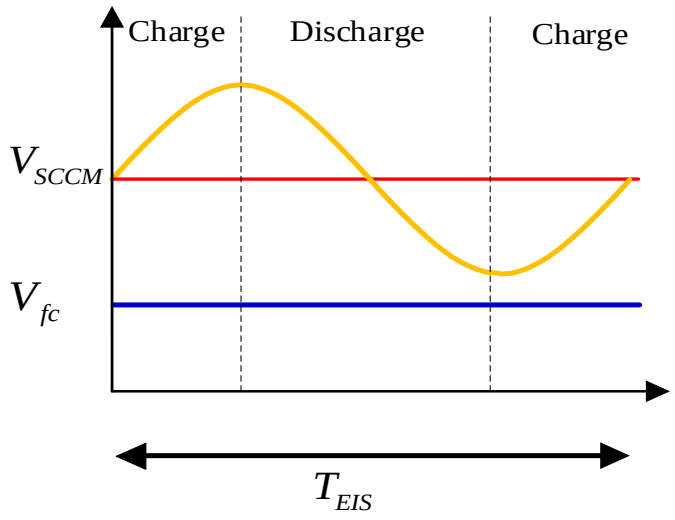

Figure 1-7 Energy exchange of SCCM

As shown in Figure 1-7 the energy exchange during operation of the EIS auxiliary converter can be written as:

$$E_{Total} = E_{Charge} - E_{Discharge} \tag{1.6}$$

where E_{Total} is zero when disregarding the losses of the system. Thus, the energy transferred during charge and discharge is of equal value.

The amount of charge transfer depends on the generated EIS switching frequency and is calculated as:

$$E_{total} = \sum_1^m \frac{E_m}{f_{EIS}} \tag{1.7}$$

$$E_{total} = \sum_1^m \frac{E_m}{f_{EIS_C}} - \sum_1^m \frac{E_m}{f_{EIS_D}} \tag{1.8}$$

where m represents the frequency of the EIS testing being performed, EIS_C is the energy demand during charging the supercapacitor string and EIS_D the energy being discharged from the supercapacitor string via SCC employed as an interface.

The detailed schematic of the switched-capacitor converter module (SCCM) is shown in Figure 1-8. The reasoning and logic behind choosing SCC with 1:9 tailored based on the case study are presented in Chapter 4. The number of supercapacitors connected in series connected to the low side of the SCC is derived in Chapter 4.

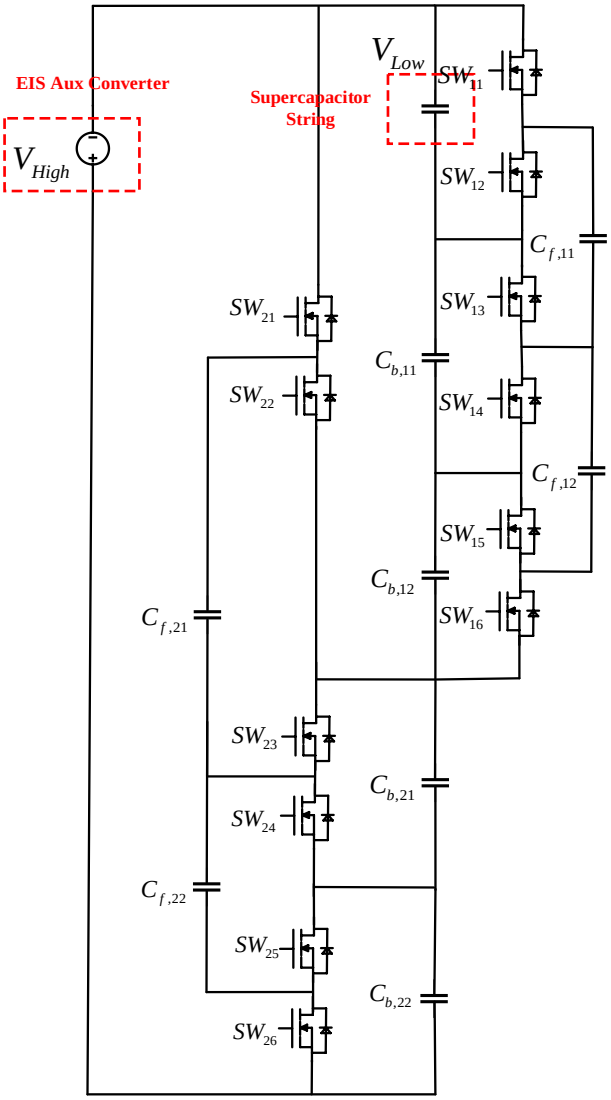

Figure 1-8 SCCM with a switched-capacitor converter of 1:9 conversion ratio.

1.7. Main Contributions and Thesis Outline

1.7.1. Thesis problem and main contributions

In this study, the energy buffer utilizing a high voltage-gain switched-capacitor converter interfaced with a supercapacitor string is proposed. Despite the fact that supercapacitors offer much higher energy density compared with electrolytic capacitors, due to the relatively low voltage rating, a bidirectional SCC is required for boosting up the voltage of the supercapacitors string to the desired voltage level to provide the voltage support for the auxiliary EIS converter to generate the EIS ac perturbations signals. Among

many existing topologies for SCC converters, the cascaded SCC is recognized as the suitable topology for this application due to requiring the least number of components which results in the most compact solution for the SCC as an interface. Also, the cascaded topology is of the common ground as the input, eliminating the need for additional circuitry for creating virtual ground. This topology also offers very low voltage ripple in the input and output side compared with many other existing solutions. In buck operation mode for SCC, voltage across the SCCM energy buffer is stepped down to charge the supercapacitor string within an allowable range without exceeding the rated voltage. The SCCM is functioning in an open-loop control system where an appropriate fixed switching frequency is chosen for this module to be able to provide sufficient energy to the bypass capacitors (output capacitors) which are similar to DC link capacitor connected to the auxiliary EIS converter to provide the required voltage support.

Among many existing SCC topologies, the cascaded SCC configuration is identified as the best suitable SCC topology, meeting the constraints of this application as listed here. 1) Full functionality (capable of providing proper bidirectional energy flow) of SCCM during buck and boost operation modes, 2) Compact in size and have the minimum number of components in total, 3) Light-weighted and relatively low cost, 4) Reduced complexity of design and implementation. As a result of the abovementioned analysis, here a compact in size SCC is proposed which results in a very compact SCCM when considering the proposed energy buffer as a whole. The selection of components including the ceramic capacitors, power MOSFETs is elaborated in detail in chapter 4.

The correlation between the FC stack, EIS auxiliary converter, and the SCCM power rating is formulated, and mathematical and simulation results are presented. Energy exchange is formulated and an explanatory graph is generated to provide a guideline for selecting the required total capacitance of the supercapacitor string to be able to provide the required energy as well as absorbing the resulted oscillations during performing the EIS testing.

1.7.2. Thesis Outline

The rest of this thesis is organized as follows.

Chapter 2 presents the theoretical statement of the thesis arguments. First, other forms of energy buffer solutions found in the literature are reviewed and the novelty of this approach to build an energy buffer module with a high buffering ratio over other existing applications is addressed. Then, it is explained what is the suitable bidirectional buck-boost converter which can be used as an interface connecting supercapacitors string with the EIS converter and the best topology towards a fully functional, cost-effective, and straightforward implementation to reduce the complexity of the whole system. As the thesis problem and research subject are introduced in sections 1.4 and 1.5, the proposed solution is elaborated in more detail.

In Chapter 3, after ensuring the practicality of the proposed solution, the theoretical analysis for the whole system is derived. For this purpose, a general description of the working principle of the EIS auxiliary converter is provided to explain the role and necessity of energy buffer in the whole system. The FC power rating and its correlation with the desirable voltage rating of the devices are introduced, and the energy exchange resulted from generating the EIS signals and absorbing the ac perturbation is explained thoroughly. The allowable voltage window for the supercapacitor string connected to the low side of the SCC is formulated and explained.

Chapter 4 presents a case study and the simulation results for the whole EIS auxiliary system and the SCCM module functionality as an energy buffer system. The voltage rating on each layer of the SCCM is investigated and differentiated from each other. The proposed energy buffer SCCM is tested under different operating points of the FC (NEXA 1.2kW) and the correlation between low EIS frequencies resulting in high oscillations and the probable limitation imposed by high EIS frequencies is explained.

Chapter 5 provides the summary of this work, and potential applications are explained and listed. The future work also is addressed to extend this energy buffer to high

power rating FC stacks for heavy duty vehicles and other applications requiring an energy buffer.

Chapter 2.

Energy Buffer Interface for the Auxiliary EIS Converter

An energy buffer module as a direct replacement for the electrolytic capacitor in the auxiliary EIS converter is proposed in this chapter. Despite the added complexity in implementation, this solution offers a much more compact instantaneous energy buffer in comparison with electrolytic capacitors. Moreover, there is a potential limitation that may occur in this application, impacting the proper functioning of this module. This limitation may happen if the discharge rate or power load demand of the connected module to SCCM is higher than the charge shuttling rate. However, by utilizing such an energy buffer module, the final solution is more compact.

2.1. Overview of High Step-Up DC-DC Converters

As discussed, the proposed SCCM energy buffer utilizes supercapacitors as the energy storage device. Considering the relatively low voltage ratings for commercially available supercapacitors (~2.5-3V) [31], there is a need for high step up dc-dc converter to increase the voltage to the desirable level defined by the load which in this case is the auxiliary EIS converter. High step-up bidirectional dc-dc converters have gained popularity due to the growing demand in many power conversion applications such as renewable energy generation with energy storage systems (ESS) [32], where the energy storage device can be battery, supercapacitor or a hybrid ESS [33]. However, for other sources such as solar photovoltaic panels and FCs, there is no need for bidirectional capability as the energy flow is unidirectional. Although, similar to supercapacitors, in FC

stacks each cell has a low voltage rating and high current, and therefore there is the need for a boost converter.

2.1.1. Inductor-based Converter

Switched-mode power supply (SMPS) dc-dc converter is developed with pulse-width-modulation (PWM) and the operation principle is by continuously storing and transferring energy in either magnetic field (inductors) or electric field (capacitors) through passive or active components such as diodes and power switches [34]. One of the commonly used step-up dc-dc converters is the boost converter, where an inductor is placed on the input side and it can operate on continuous conduction mode (CCM) or discontinuous conduction mode (DCM). The inductor is known to be one of the largest components in terms of volume in this topology and the size of the inductor can be determined based on the control algorithm and topology [34]. The actual sizing is a trade-off that needs to be done realistically. Therefore, the existence of the inductor significantly increases the size and volume and requires larger electromagnetic interference (EMI) filters as a result of the presence of an electromagnetic field in this converter. Also, similar topologies mostly have a minimum requirement of an implemented feedback control loop that adds control and implementation complexity, cost, and decreases the reliability of the converter by taking into account the correlation between increasing the number of components and the chance of failure.

Although, isolated converters have advantages such as decoupling the input and output which adds more reliability to the system [35], the necessity of this feature is not recognized for the auxiliary EIS converter as it is not used on regular bases and mostly is scheduled to be functioning for approximately a few minutes window with a relatively low power rating to inject and process the ac perturbation with different frequencies. Besides the aforementioned justifications, this auxiliary EIS converter module consists of a half-bridge (HB) converter which is assigned to generate the EIS perturbation and interpret the incoming data, therefore, the auxiliary EIS converter system as a whole is considered to be an isolated module. Non-isolated dc-dc converters, generally, as a result of their broader application range, simpler implementation, and overall compactness due to the elimination

of magnetic coupling are more subjected to research [34]. By taking into consideration the requirements of this application explained in the previous chapter such as compactness, and cost-effectiveness, non-isolated converters are selected for further research.

There are a large number of inductor-based SMPS converters that can perform in step-up mode. several known ones such as conventional boost (Figure 2-1), SEPIC, and Cuk converters which operate through regulating the required magnitude of current by controlling the power switches via the PWM signal. Other types of SMPS converter which provide galvanic isolation are such as Flyback, Forward, push-pull, half- and full H bridge [36] converters which contain an inductor split into two transformers. Having inductor in the converter contributes to an increase in size of the converter not to mention that requirement for control system which contains the sensor circuitry and embedded control algorithm into the microcontroller to control the power switches via generating appropriate PWM signal. These requirements add complexity to the implementation of the converter. Therefore, having a power inductor and/or transformer in the converter, adds cost, complexity to control algorithm and implementation of the converter, and increases the size of the converter which questions the compactness as the first requirement of this application. In order to be able to reduce the size of the inductor, many topologies resulting from a combination of different topologies such as SCC with other types of power conversion methods are proposed in academia as well as industry.

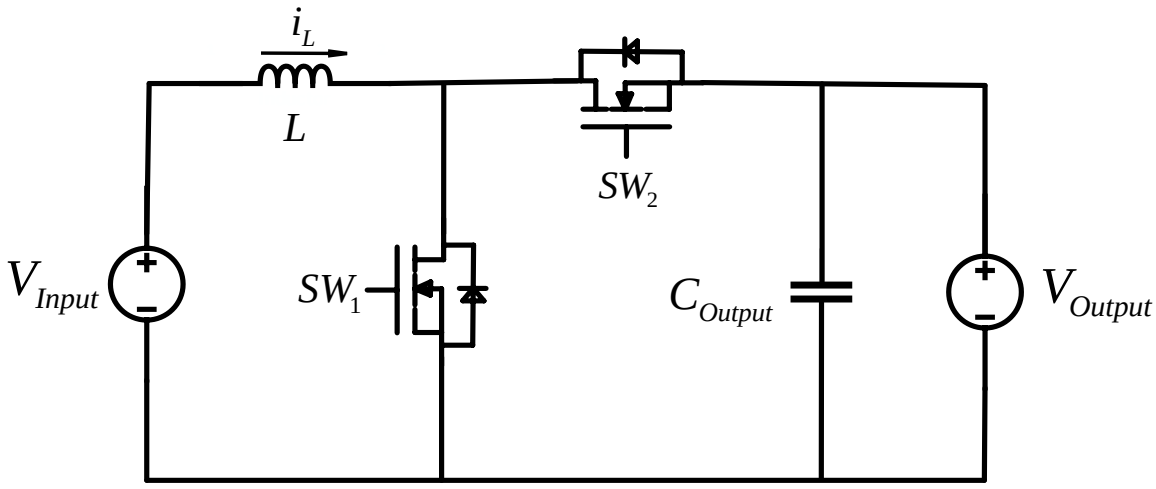

Figure 2-1 Conventional synchronous boost converter

2.1.2. Switched-Capacitor Converter

Development of the switched-capacitor (SC) converter stems from the rapidly increasing demand for a small-form-factor (e.g. compact and light-weighted), high efficiency, and low-cost converters which are in general desirable factors for many applications. The working principle of SCC relies on charge shuttling (charge redistribution or charge sharing) between the flying capacitors and bypass capacitors in the network circuit shown in Figure 2-2 through power switches controlled with nonoverlapping PWM signals [30]-[37] depicted in Figure 2-3. In addition to the relatively simple operating principles for SCCs, as mentioned previously, it is a cost-effective solution due to eliminating the need for an expensive and bulky microcontroller needed for the inductor-based converter. Whereas for SCCs, mostly a small and inexpensive clock can govern the power switches to shuttle the charge via complementary PWM signals [38]. To mention another advantage of SCCs is using relatively lower blocking voltage switches leading to a substantial decrease in the Total Device Power Rating (TDPR) of the system [39] which contributes to compactness and generally lower price. For applications requiring a high-resolution output voltage, an interleaved SCC was proposed in [40]. However, the proposed method requires a large number of components including power inductors, leading to a large SCC with high blocking voltage. The total size of SCCs can be reduced by using diodes as a single quadrant switch instead of controlled power switches such as MOSFET. By doing so, the size of the SCC drastically decreases and results in a much smaller solution [41]. Although, due to the utilization of diode, the SCC is not able to perform bidirectional energy flow. In addition to that, the voltage drop for diodes are in general higher than the switching losses and conduction losses ($R_{DS}\,(ON)$) of MOS switches leading to a less efficient dc-dc converter which essentially leads in alteration in conversion ratio. A SCC with Fibonacci arrangement was proposed in [42]. Although this topology uses relatively fewer capacitors in its network but instead uses a much higher number of power switches to create a path for the charge to shuttle. As a result of the increase in the number of power switches, the required number of switch gate drivers to run ON and OFF the switches increases, leading into a large SCC design, not to mention the increase of capacitance in each stage to be able to provide sufficient energy in presence of high output power demand. A well-known topology similar to the proposed hybrid SCC

in [43] is an SC voltage doubler. Although this topology offers a straightforward implementation and control strategy, it is unable to reach high conversion ratios. Therefore, to reach higher conversion ratios, cascading multiple of them is required. Although, cascading SC voltage doubler converters does not give us the flexibility of achieving any conversion ratios, only integers resulting from formula 2^n (n is the number of cascaded voltage-doublers). The PEM FC technology is a FC stack with a relatively lower operating temperature, but it can reach up to 100 Celsius while operating. Therefore, considering the leakage current of inductors increases by temperature rise [44], leading to converter's efficiency degradation[45]. Therefore, eliminating inductors from this design can be beneficial for EV applications, in general.

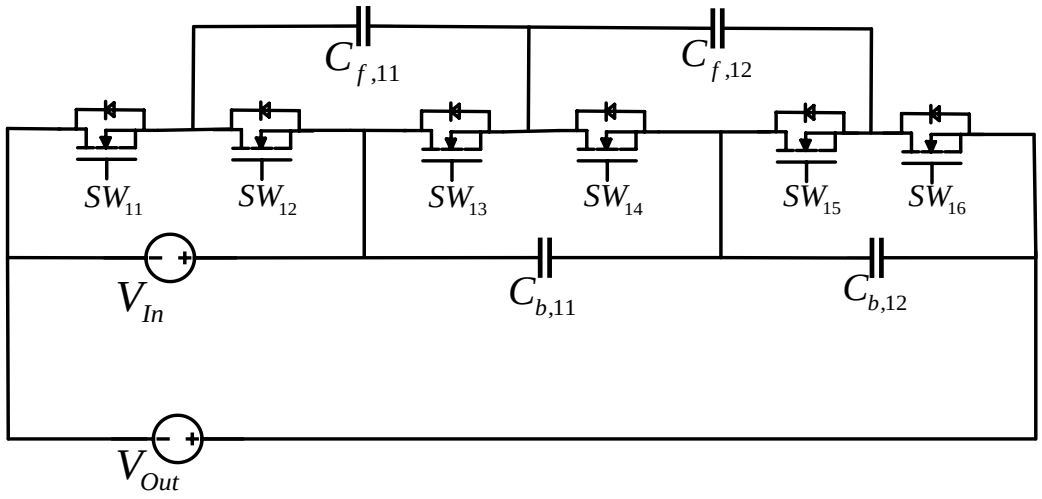

Figure 2-2 Ladder type switched-capacitor converter with 1:3 conversion ratio

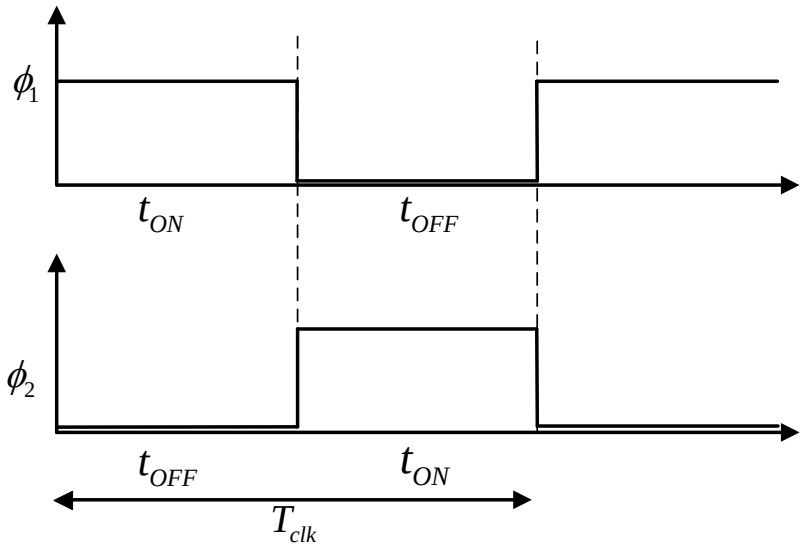

Figure 2-3 Switched-capacitor control signals

Although, SCC can achieve high efficiency owing to no need for inductors (eliminating magnetic losses) [30], the efficiency is strongly impacted relating to the conversion ratio [27] and [46]. Another shortcoming of SCCs is that many of the existing topologies are not capable of reaching a precise resolution and a well-regulated output voltage in the presence of wide load current and voltage variation [38].

2.1.3. Hybrid Switched-Capacitor Converter

A highly-efficient resonant switched-capacitor converter is proposed in [46] (shown in Figure 2-4) and [47] which are capable of boosting the input voltage and achieving bidirectional energy flow by controlling the sequence of the switches governed by a pair of complementary PWM signals. This topology reaches step-up (step-down) bidirectional energy flow by employing an LC tank, consisting of a large number of components. The efficiency of the system is stated to be above 90% over a wide range of conversion ratios. Another hybrid switched-capacitor converter was proposed in [48] by modifying the deployment of the main power switches and placing the switched-capacitor at the output of the high-voltage side, requiring additional circuitry and control. A high energy-

efficiency hybrid SCC with a continuous conversion ratio is proposed in [46], as shown in Figure 2-4, which requires current sensing circuitry to achieve zero-current switching (ZCS) in order to mitigate the losses of the SCC due to their nature of hard switching. Also, to mitigate the switching losses of SCC in ladder topology, a resonant SCC was proposed in [49]. Despite the need for using inductors in this topology, the size for the inductors are relatively smaller compared to other hybrid SCCs. However, the proposed topology requires a dramatically large number of components to reach a high conversion ratio, therefore, results in a bulky solution and the need for additional circuitry and control algorithm. Although most of the abovementioned solutions offer a good deal of efficiency, high voltage gain, and minor voltage variation, they are constructed from a large number of components especially power inductors, required control algorithm implementation, increase in cost, and complex implementation process.

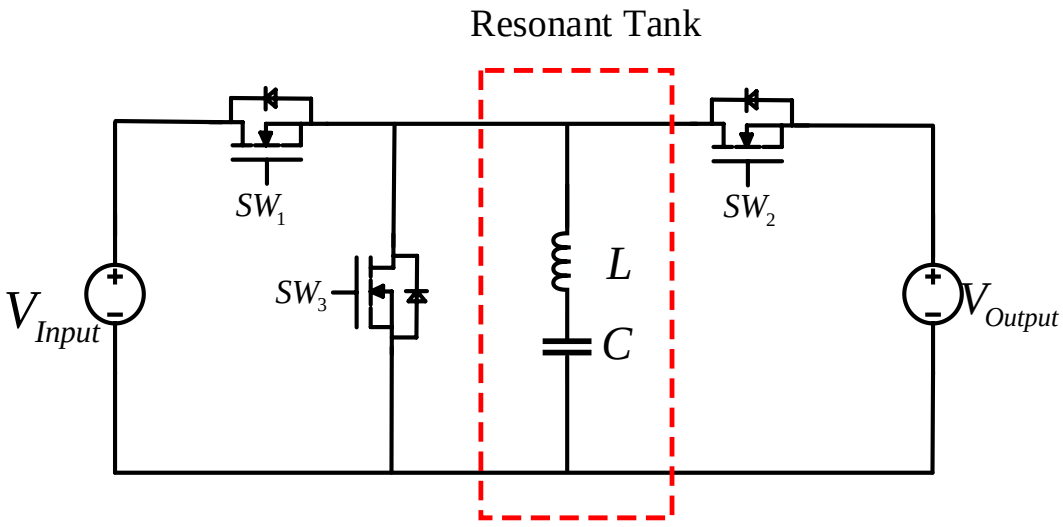

Figure 2-4 Resonant switched-capacitor converter

2.2. Reasoning for Choosing the SCC as the Energy Buffer Interface

To be able to choose the suitable dc-dc converter for this application, let us revisit the constraints of this application stated below:

I. High voltage gain and bidirectional energy flow

II. Compact in size and light-weighted

III. Relatively inexpensive and durable

IV. Scalability, flexibility in conversion ratio, and implementation process

V. High power deliverability and preferably energy-efficient

In general, the SCC meets all the listed application constraints and factors listed above. However, SCCs explained in the literature review have many different topologies and networks of switches and capacitors. Therefore, a comparison between the existing topologies to take one step further and identify the best solution is done in this section. It is worth mentioning that the effective power density and compactness of any specific design depends on the topology of the SCC [50]. Moreover, most conventional SCC operating in the open-loop control system have good capability of operating under the no-load condition which essentially eliminates the need for implementing a dumping resistor that potentially adds complexity to the converter design [51].

2.3. Switched-Capacitor Converter Topology Selection

Historically SCCs are used mostly for low power rating applications (<100mW), but recent development and utilization of SCC on higher power rating applications such as [28] and [39] demonstrate the capability of this converter type in performing on higher power rating applications. The aforementioned benefits in the previous chapter in utilizing SCC over other existing solutions have motivated the selection of SCC for this research [50]. The energy density of the SCC depends largely on its topology [39]. Therefore, an appropriate selection of SCC topology from the existing methods can significantly help to reduce the size and resolve potential limitations explained in the following chapter. Thus, in this section, the comparison between some of the previously introduced topologies for SCC is discussed to provide the guideline for choosing the most suitable one for this application over the other topologies.

Table 2-1 Feature comparison of different SCC topologies

SCC Type	Component Count	Voltage Stress	Shortcomings
Voltage Doubler [27]	Medium	Medium	Unable to reach any conversion ratio and large component counts and efficiency drops.
Fibonacci [42]	Medium	High	Unable to reach any conversion ratio and large TDPR.
Ladder Type [49]	High	Low	Large component count and efficiency drop for high conversion ratios
Multilevel [52]	Medium	Medium	Cell imbalanced and not some common ground in some configurations
Series-Parallel [53]	Very High	High	A large number of components and relatively lower efficiency for high conversion ratios
Cascaded [28]	Low	Medium	The possible drawback for cascading multiple SCs

2.4. Control Principle of Switched-Capacitor Converters

As briefly explained in previous sections, SCCs are usually controlled with a complementary pair of PWM signals to harmonize the charge transfer from one capacitor to another. Most of the established SCCs require only 2 complementary PWM signals with 50% duty cycle [30] and [54]. However, some other topologies utilize more than 2 PWM gating signals or an unequal duty cycle [55] to achieve different objectives such as ripple reduction and power quality improvement. The shown waveforms in Figure 2-5 in [44] is provided to demonstrate the working principle of the SCC.

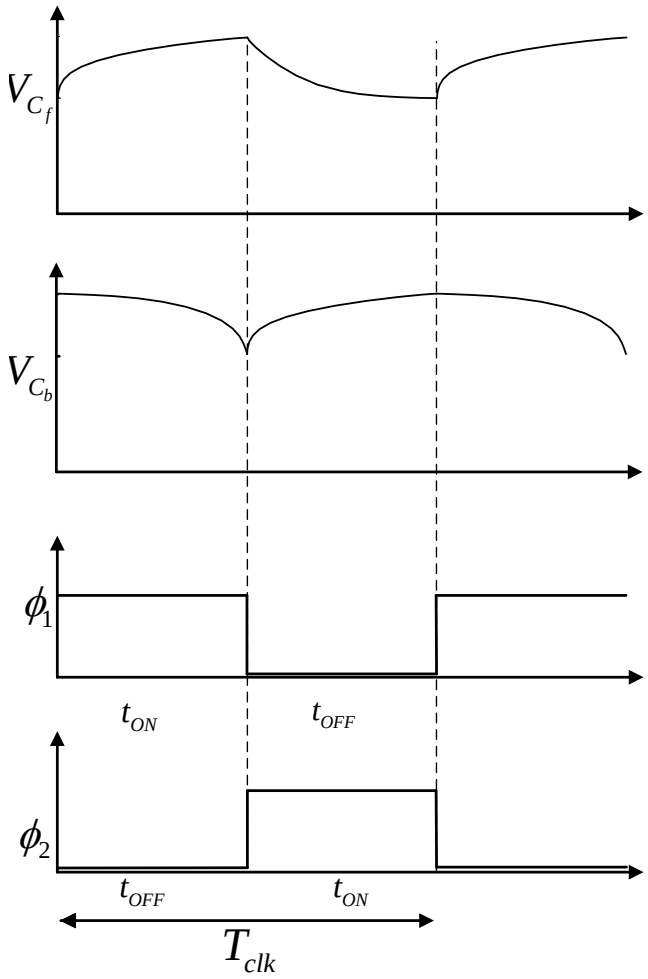

Figure 2-5 Complementary pair of PWM signal and capacitors waveforms

Power switches in the SCC network fall into two groups where each group is controlled with one PWM signal. Grouping switches are merely based on the arrangement of the switches and capacitors but the concept is to transfer the energy by creating a path for current to flow from one source to another. Unlike inductor-based converters that by modulating the input dc voltage applied to one side of the inductor, to convert the output voltage, SCCs save and transfer charge in the form of voltage across the flying capacitors [50].

One of the distinct advantages of SCCs as compared with other dc-dc conversion methods is their straightforward control algorithm, although there has been the

development of different circuitries and control algorithms [34], [38], [39], [56]-[57] to improve the out power quality and resolution of the SCC for applications requiring accurate voltage level such as providing power to a MCU.

2.5. Cascaded Switched-Capacitor Converter

The cascaded SCC consists of more than one SCCs connected in cascade forming a converter with higher conversion ratios. Based on the placement and connections of the SCC, any integer number for the conversion ratio can be obtained, giving great flexibility to achieve any desirable conversion ratio [28]. For instance, a cascaded SCC is presented in Figure 2-6 with 1:6 conversion ratio. A more general analysis for SCC circuits is presented in the following section with an SCC of 1:3 which is a part of the 1:6 cascaded SCC as shown below.

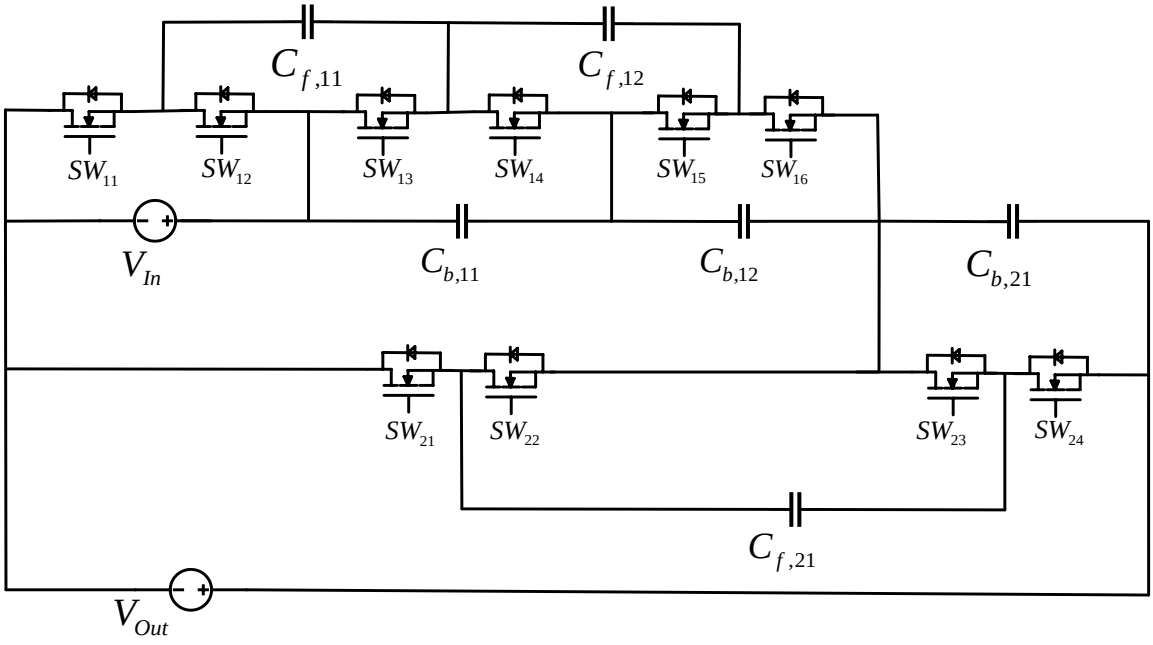

Figure 2-6 Cascaded SCC with 1:6 conversion ratio

2.5.1. Equivalent Circuit Analysis for SCC

Here a general working principle of SCC and its circuit analysis with KVL is presented. The depicted SCC in Figure 2-7 offers a 1:3 conversion ratio.

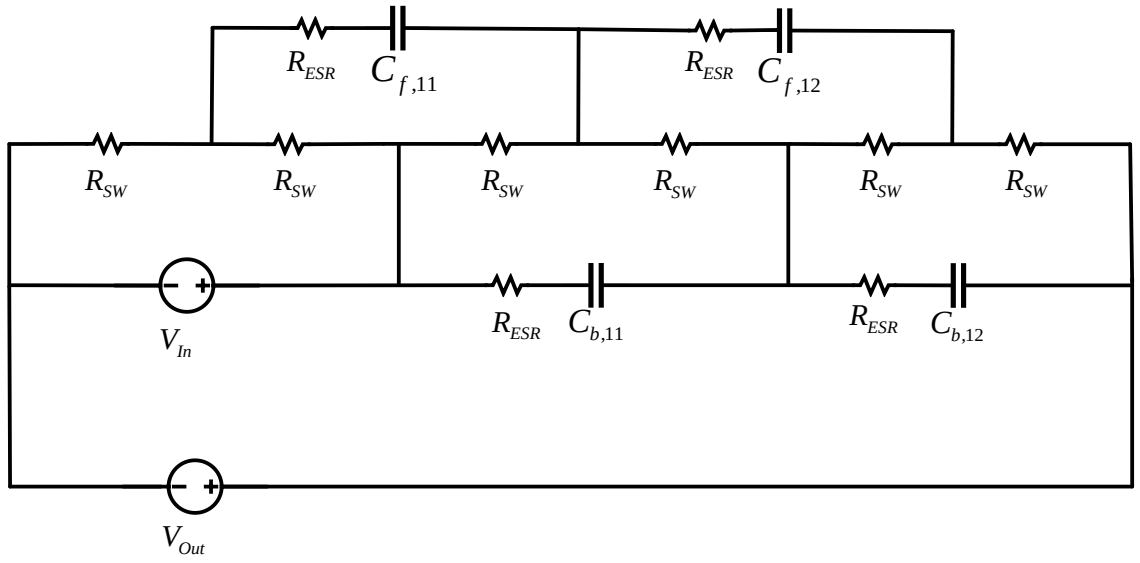

Figure 2-7 SCC with 1:3 conversion ratio

Disregarding the warm-up stage of the SCC, the equations can be written as below:

$$V_{In} = V_{C_{b,11}} = V_{C_{b,12}} \tag{2.1}$$

$$V_{Out} = V_{In} + V_{C_{b,11}} + V_{C_{b,12}} \tag{2.2}$$

$$V_{Out} = 3V_{In} \tag{2.3}$$

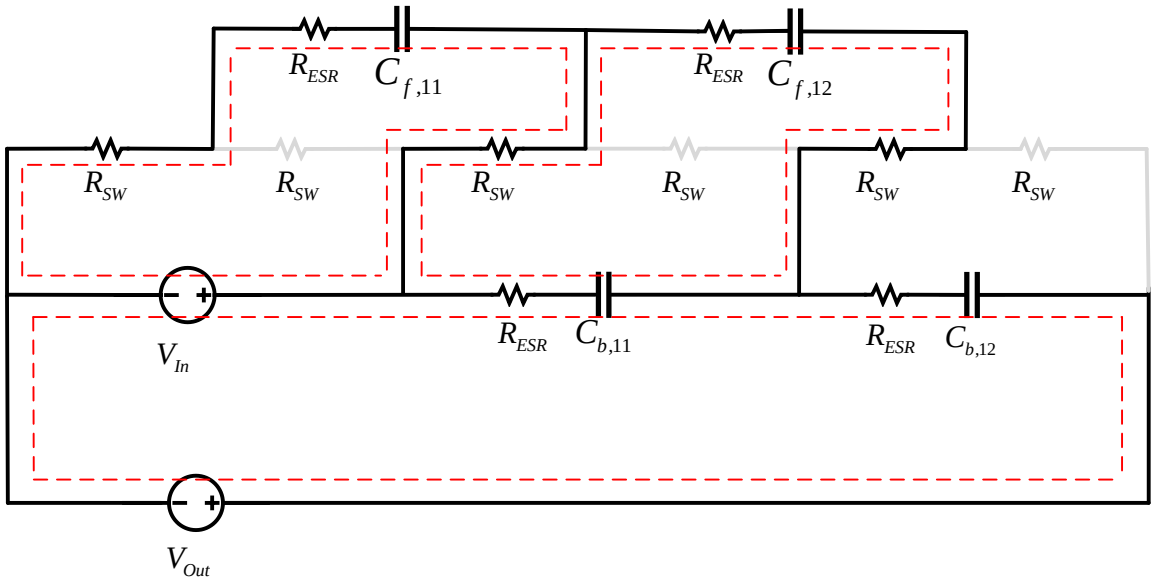

Figure 2-8 SCC with 1:3 conversion ratio in Phase 1

In phase 1 ($\emptyset_1$), V_{in} is placed in parallel with $C_{f,11}$ (with respect to charge sharing principle that 2 capacitors connected in parallel are of the same voltage) resulting in (2.4). As a result of small ESR for the ceramic capacitors, the voltage drops across each R_{ESR} are neglected. At the same time, the first bypass capacitor (output capacitor) is in parallel with $C_{f,12}$ shuttling the charge to the second flying capacitor resulting in (2.5).

$$V_{In} = V_{C_{f,11}} \tag{2.4}$$

$$V_{C_{b,11}} = V_{C_{f,12}} \tag{2.5}$$

Bypass capacitors are being constantly discharged through V_{Out} while flying capacitors are shuttling the charge from the input to the bypass capacitors.

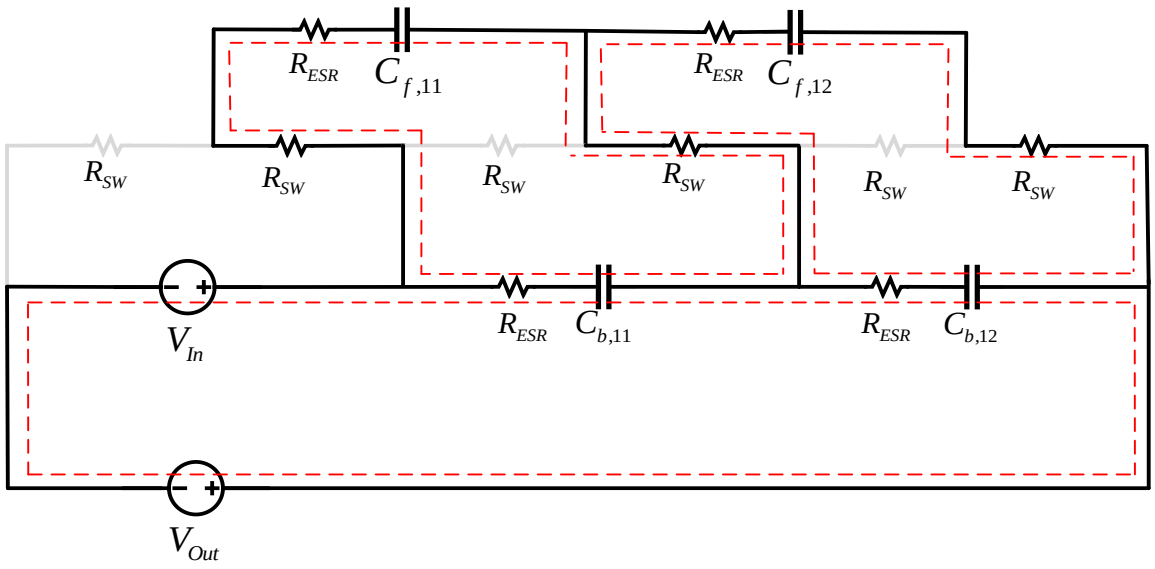

Figure 2-9 SCC with 1:3 conversion ratio in Phase 2

In this phase ($\emptyset_2$), the first flying capacitor is in parallel with the bypass capacitor $C_{b,11}$ to shuttle the charge obtained in phase 1 to the bypass capacitor. This process is repeated for the flying capacitor $C_{f,12}$ shuttling the charge to $C_{b,12}$.

$$V_{C_{f,11}} = V_{C_{b,11}} \tag{2.6}$$

$$V_{C_{f,12}} = V_{C_{b,12}} \tag{2.7}$$

2.6. Component Selection

Due to the existing limitations such as voltage rating, capacitance, and parasitic elements on commercially available components, selecting appropriate components for SCCs plays a crucial role in designing the SCC. The SCC here contains two fundamental components power switch and capacitor and a gate driver to enable the system to perform precise and consistent turning on and off the switches. As mentioned before and stated in [50], there are other factors we can have control over. Those factors are the switching frequency and duty cycle of the SCC. However, when designing the SCC, having the power switches with a low $R_{DS}(ON)$ and capacitors with low R_{ESR} is crucial. Also, the effective and relatively large flying capacitor capacitance significantly helps to ensure an appropriate

charge shuttling rate which implies the functionality of the SCC [50]. In general, SCCs with large capacitance and low MOSFET resistance are capable of reaching the highest efficiency and known to be a good practical design [37], as the round trip efficiency of the capacitors correlated with the voltage ripple. Therefore, the larger the capacitance, the less ripple is resulted, leading to a more efficient SCC.

2.7. Total Device Power Rating

Total Device Power Rating (TDPR) is a suitable evaluation metric for the realization of the cost and size of any converter. TDPR is the summation of the components used for a specific design. The formula below exhibits the derivation of the TDPR value for SCC:

$$TDPR_{SCCM} = \sum_1^x C_{bx} + \sum_1^x C_{fx} + \sum_1^x SW_x \tag{2.8}$$

where x is the number of components and its positioning in the SCC network. For example, if a capacitor is located in the first level the second layer of a cascaded SCC, it will be annotated as $C_{f,21}$.

This value can be individually calculated for each component as well as done for the entire existing components in the converter.

2.8. Initial Design

In this section, the determination of switching frequency and the capacitance of the capacitors in the SCC network are discussed. This provides a guideline for designing this specific SCC topology and thereafter, when the factors are chosen, based on the availability and potentially the cost-effectiveness of the components in the market, the design can be fulfilled afterward.

As shown in Figure 2-7, the SCC topology used in this application consists of two groups of capacitors named bypass capacitors and flying capacitors. To differentiate these two capacitors from each other, the main string of capacitors connected to V_{In} are bypass capacitors where they are connected to the same ground as the input and annotated as C_{bx}.

On the other hand, the floating capacitors that are constantly changing their positioning based in the switching frequency and the duty cycle (usually 50%) orchestrating the switches are named the flying capacitors annotated as C_{fx}.

Let us formulate the correlation between the switching frequency and the capacitance of the bypass capacitors in the SCC ($i_{discharge} = C_{bypass}\frac{\Delta v}{\Delta t}$)

$$C_{bypass} = \frac{\Delta t\, i_{discharge}}{k\, V_{bypass}} \tag{2.9}$$

where C_{bypass} is the bypass capacitors' capacitance, and $i_{discharge}$ is the discharged current associating with the output power load demand. k is the allowable ripple represented in percentage which is derived based on the output power demand, and V_{bypass} is the voltage across the capacitor associating with their voltage stress.

On the other hand, referring to the abovementioned control strategy with respect to the duty cycle of this SCC control algorithm, determination of capacitance for the flying capacitors are derived as below:

$$C_{flying} = \frac{1}{D}\,\frac{\Delta t\, i_{discharge}}{k\, V_{bypass}} \tag{2.10}$$

where D is the duty cycle depending on the topology of the SCC (factor of 2 for the cascaded SCC). Although, it is recommended to choose the higher value for flying capacitors to be able to shuttle more energy to the bypass capacitors to assure the appropriate functionality of the SCC [50].

2.9. Power Switch Gating Driver Selection

MOSFET Gate Drivers converter logic signals to a higher voltage and current levels to drive MOSFET gates ON and OFF with fast response times. For instance, MOSFET drivers can be used to convert a 3.3 or 5V low-current signal generated by an MCU to a larger voltage with a much larger current as a drive signal to change the state of a MOSFET state from ON to OFF. There are two possibilities for choosing gate driver, named low side

and high side drivers. Low side gate drivers are used when the switch is directly connected to the common ground, whereas for the high side gate driver, the switch is floating and not connected to the same ground.

2.9.1. High Side

For instance, as explained previously, based on the positioning of the power switches, it can be determined whether the switch needs a high side gate driver or a low side one. As depicted in Figure 2-10, the power switch is not connected to the common ground and is floating, changing its path according to the receiving gating signals. Therefore, a high side gate driver is needed for the switches to be able to turn ON and OFF appropriately.

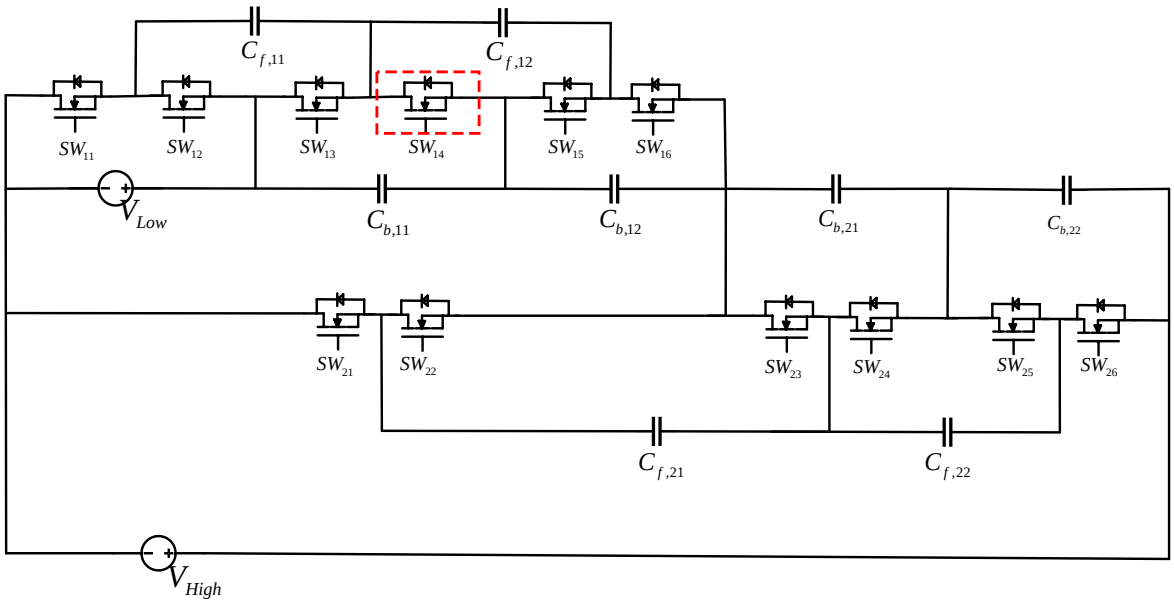

Figure 2-10 Power switch positioning in the SCC network

2.10. Capacitor Characteristics Modeling

Supercapacitors and ceramic capacitors are not considered as linear capacitors as some nonlinearity due to many deterministic factors are observed in many publications such as [18], [58]-[59]; therefore, the capacitance can be realistically calculated from a

good model. The observed nonlinearity in the abovementioned capacitors is represented as:

$$C = \frac{Q}{V} \tag{2.11}$$

where C is the capacitance of the capacitor, Q is stored charge, and V is the voltage.

$$i = \frac{dQ}{dt} = Q' \tag{2.12}$$

After rearranging (2.12), the linear and non-linear terms can be separated as below:

$$i = C'V + V'C \tag{2.13}$$

The first term $C'V$ is omitted from the equation if the capacitors are considered to be linear (Helmholtz capacitance), but in practice, capacitance varies, and changes based on certain factors. For instance, charge redistribution causes some increase in the capacitance of supercapacitors in medium or long-term discharges. Whereas this could lead to a decrease of capacitance when charging the supercapacitor. Also, the applied voltage across the terminal of the capacitor can have an impact as explained here. Therefore, for a better modeling $C'V \neq 0$.

2.10.1. Voltage-Dependant Capacitance

Ceramic capacitors and supercapacitors have the voltage dependency characteristic which needs to be taken into account when designing for a specifically required capacitance. In this work, both ceramic capacitors in SCC and supercapacitors as an instantaneous source of energy being charged and discharged during one full cycle of the EIS testing present. It is worth mentioning this phenomenon associated with the actual voltage being applied on the terminal of each type of capacitor.

Ceramic capacitors have negative voltage dependence capacitance coefficient whereas for supercapacitors, this factor is of a positive value. This value can reflect as millivolt for lower capacitance and as the capacitance and voltage rating of the capacitor increases, it reaches higher voltage levels.

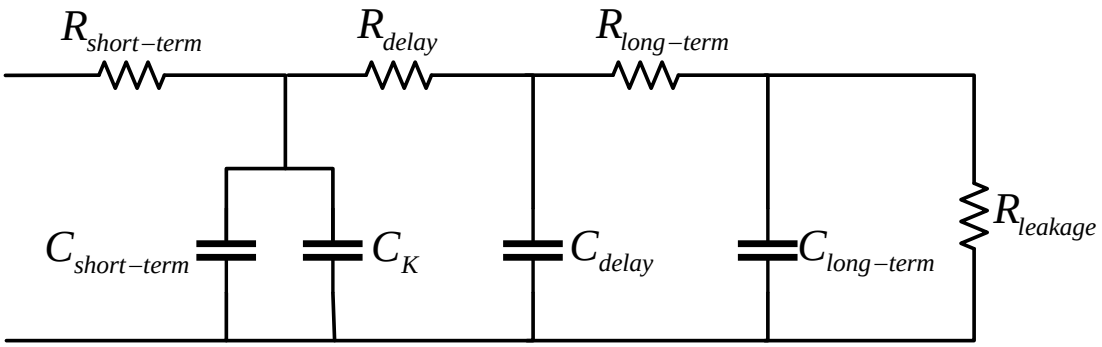

Figure 2-11 Zubieta model for Capacitor

The voltage-dependent factor C_k in Figure 2-11 is shown by modeling the capacitor as a ladder RC circuit. This coefficient is usually provided in the datasheet of the ceramic capacitor manufacturer. For example, as stated in [37], when using the Z5U type of ceramic capacitor, the calculated capacitance with considering the voltage-dependent coefficient leads in 50% decrease in the total capacitance as compared with X7R under the same working condition. And this shows the importance of a model as an appropriate tool to calculate the actual capacitance. This capacitance deviation which is the result of voltage depended coefficient as explained in Figure 2-11 is shown in Figure 2-12 [59] for better visualization.

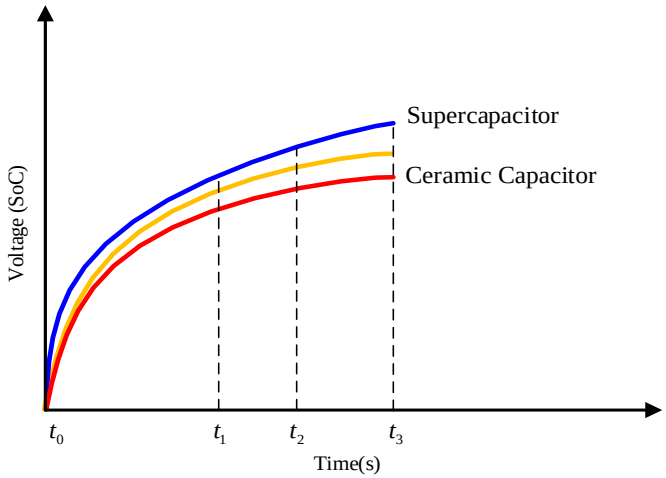

Figure 2-12 Depiction of supercapacitor and ceramic capacitor capacitance with the voltage-dependent coefficient

2.11. Conclusion

A general overview of different types of dc-dc converters was presented in this chapter. Among different possibilities to design a bidirectional high voltage gain dc-dc converter, the SCC was chosen due to its capability and uniqueness to meet the requirement of designing an energy buffer for auxiliary EIS converter. Thereafter, multiple existing SCC topologies were compared and the cascaded SCC was identified and selected for implementing the energy buffer interface for the auxiliary EIS converter. The objectives determining the selection of cascaded SCC were listed and cross-referenced to give the reasoning for selecting the SCC.

After selecting the suitable SCC, a general circuit analysis, component selection, switching frequency, and capacitor capacitance determination, and capacitor modeling was discussed towards designing the parameters for the SCC.

It is concluded the selected SCC with considering the discussed factors is capable of acting as an interface between supercapacitor string and the auxiliary EIS converter. It is to boost up the voltage to provide the required energy needed for the auxiliary EIS converter to generate the AC signals and to step down the voltage when measuring the ac perturbation and absorbing them with the supercapacitor string.

Chapter 3.

Design Details and Energy Buffering Principle

In this chapter, the requirement for enabling the auxiliary EIS converter to generate ac perturbation is discussed. The energy transfer which is resulted from performing EIS is described, and the working principle and role of the proposed energy buffer are analyzed. The role of supercapacitor string capacitance is formulated, and an explanatory graph is provided.

3.1. Introduction

An auxiliary EIS converter decoupled from the main power processing unit is proposed and developed in [15] and [16] offering a dedicated EIS converter option. However, the EIS converter is a dc-dc converter requiring the energy to be dumped through a dumping resistor at the load side. The innovative idea of having a separate dedicated EIS converter brings several benefits such as:

I. As a plug and play module that provides great flexibility
II. Decoupling the main power conditioning converter (PCC) from perturbation generating device
III. The auxiliary EIS converter needs to be sized to process the ac perturbations, thus, resulting in a compact module

The benefits of using the proposed energy buffer named as SCCM with utilizing supercapacitors as an energy storage device interface with an SCC is listed below:

I. Eliminating the need for using bulky electrolytic capacitors, resulting in a more compact solution

II. Not having the lifetime problem of electrolytic capacitors as the life expectancy of supercapacitors is higher than electrolytic capacitors

III. Ability to tailor the design and customize it based on the requirement of the application

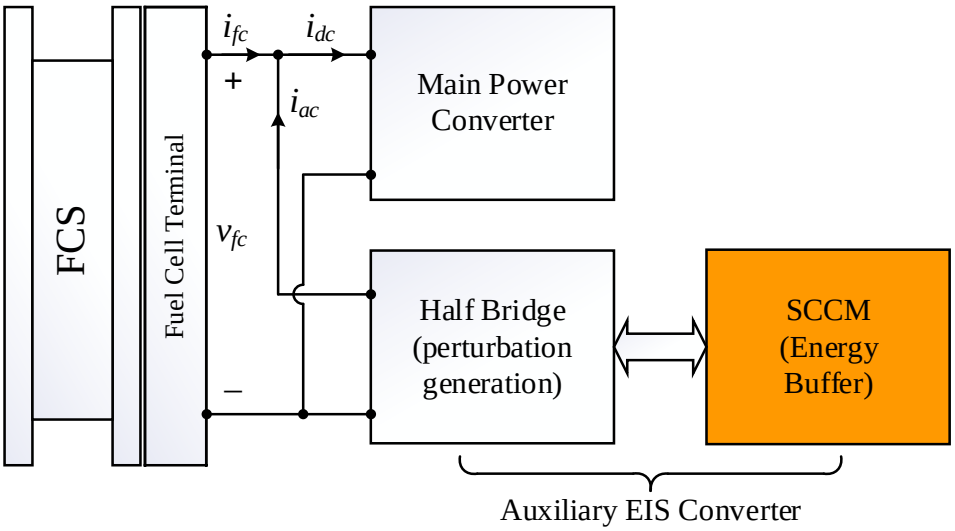

Figure 3-1 Overview of the auxiliary EIS system with SCCM

3.2. Overview of the Proposed System

An overview of the auxiliary EIS converter with the proposed energy buffer SCCM is shown in Figure 3-1, consisting of controlled and uncontrolled parts. The auxiliary EIS converter is assigned to generate the ac perturbation signals and the proposed SCCM which is the focus of this work is to provide and absorb (charge and discharge) the resulted energy to the SCCM during buck/boost operation modes. Eliminating the resistive load needed to absorb the oscillations resulted from EIS leads into a more compact result, with a decrease

in cost, simplify the implementation and control complexity, no need for a heat sink, and potentially dedicated thermal management. This auxiliary converter works as a reactive power generator to inject ac perturbation into the fuel cell stack to perform EIS excitation. The resulting oscillations from EIS are absorbed by the SCCM. The supercapacitor string connected to the low voltage side of the SCC provides the required voltage support during boost operation while maintaining the voltage above the voltage of the FC stack, i.e., $V_{fc} < V_{SCCM}$. As the proposed auxiliary converter connected with SCCM is to perform the EIS excitation and absorb the resulted oscillations, one possible choice is to place a capacitor across the terminals of the half-bridge auxiliary EIS converter. This is extended here by replacing the capacitor with a high voltage gain bidirectional SCCM which functions similarly to any instantaneous energy storage device. The components on the SCC are sized to withstand the magnitude of the ac perturbation and the resulted ripples. The SCC component sizing and the suitable number of supercapacitors connected in series and the total capacitance are presented in this section.

3.3. Switched-Capacitor Converter Design

As previously mentioned, one of the important advantages of an auxiliary EIS converter is its decoupling state from the main power converter; thus, it only needs to be sized to process the EIS perturbations injected into the FC stack. Normally, the ac current perturbation is set to 10% (to assure the integrity of the EIS signals) of its dc operating point and is expressed as:

$$i_{ac} = 0.1 I_{fc} \sin(\omega t) \tag{3.1}$$

where I_{fc} is the magnitude of the fuel cell output current and ω is the angular frequency of the ac perturbation. A simplified model of an FCS is shown in Figure 3-2 using the Randle's equivalent circuit.

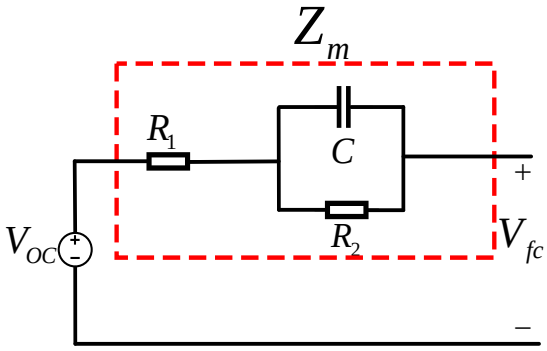

Figure 3-2 Fuel cell stack model with Randle's circuit.

After applying the EIS signals, the output voltage to be processed by the EIS auxiliary converter is composed of both dc and ac components. The ac component is denoted as P_{ripple} due to the existence of the ac signal and dc bias. From the simplified model of a fuel cell which is consisting of an open circuit voltage V_{OC} and the unknown internal impedance of the fuel cell denoted by Z_m ($Z_m = R_1 + \frac{R_2}{1+j\omega CR_2}$) and is intended to be measured by performing EIS. Therefore, by reorganizing (3.2) the output voltage can be written as (3.3). The internal resistance denoted as Z_m is related to the real value of the internal resistance of FC.

$$v_{fc} = V_{OC} - V_{Z_m} \tag{3.2}$$

$$v_{fc} = V_{OC} - Z_m\left(I_{fc} + i_{ac}\right)$$

$$= V_{OC} - (R_1 + R_2)I_{fc} - \left(R_1 + \frac{R_2}{1+R_2 j\omega C}\right) i_{ac} \tag{3.3}$$

where $V_{OC} - (R_1 + R_2)I_{fc}$ is the dc component of the fuel cell output voltage and $-\left(R_1 + \frac{R_2}{1+R_2 j\omega C}\right) i_{ac}$ is the ac component.

The output power of the fuel cell is written as:

$$P_{fc} = (V_{OC} - V_{Zm})(I_{fc} + i_{ac}) \tag{3.4}$$

$$P_{fc} = I_{fc}\left(V_{OC} - (R_1 + \mathrm{R}_2)I_{fc}\right) - 0.1Z_m I_{fc}^2 \sin(\omega t) + 0.1\left(V_{OC} - (R_1 + \mathrm{R}_2)I_{fc}\right)I_{fc} \sin(\omega t) - 0.01Z_m I_{fc}^2 \sin^2(\omega t) \quad (3.5)$$

After eliminating the dc and double frequency components, the P_{ripple} is written as:

$$P_{ripple} = -0.1(R_1 + \mathrm{R}_2)I_{fc}^2 \sin(\omega t) + 0.1P_{dc} \sin(\omega t) \quad (3.6)$$

As explained previously, the required number of supercapacitors connected in series in the low side of the SCC is required for the design of the SCCM. To calculate this value, the power rating of the FC stack is required. Also, the total power transfer needs to be calculated for the capacitance selection section to ensure the appropriate operation of the SCC during buck and boost operations.

After rearranging (3.5), the P_{fc} is written as:

$$P_{fc} = P_{dc} - 0.1(R_1 + R_2)I_{fc}^2 \sin(\omega t) + 0.1P_{dc}\sin(\omega t) \quad (3.7)$$

Therefore, after assuming the internal resistance of the FC is equal to zero, the (3.6) can be simplified as (3.8) which represents the peak power:

$$P_{ripple\,max} = 0.1P_{dc}\sin(\omega t) \quad (3.8)$$

where P_{ripple} is the exchanged power during the charging and discharging of the SCCM energy buffer. As mentioned at the beginning of this section, the EIS auxiliary converter needs to be sized and capable of withstanding P_{ripple}. The fuel cell current (I_{fc}) and dc power (P_{dc}) is determined by the dc operating point of the fuel cell, while Z_m is to be determined by performing the EIS excitation.

3.4. Supercapacitor String Capacitance

The ac component is expected to be absorbed by the supercapacitor string during buck operation of the SCCM. Ignoring the energy losses of the EIS converter and the SCCM energy buffer, the energy stored in the proposed system considering all energy storage devices is written as:

$$E_{Total\ SCCM} = E_{SC\ String} + E_{SCC\ Converter} \tag{3.9}$$

where $C_{SC\ String}$ and $V_{SC\ String}$ are the total capacitance and the voltage of the supercapacitor string attached to the low side of the SCC and C_{SCC} and V_{SCC} are corresponding with the capacitors deployed in the SCC module. Acknowledging the fact that $C_{SC\ String} \gg C_{SCC}$, therefore, the stored energy on capacitors in SCC can be neglected for energy stored.

SCCM consists of a supercapacitor string that is interfaced with an SCC with a 1: n conversion ratio. Therefore, the voltage of the SCCM supplied by the supercapacitor string can be written as (3.10) in the form of the total energy stored in supercapacitor string as (3.13).

$$V_{SCCM} = n(V_{SC} + \Delta v_{sc}) \tag{3.10}$$

$$V_{SC} = \frac{V_{SCCM}}{n} + \frac{\Delta v_{SCCM}}{n} \tag{3.11}$$

$$V_{SC} = \frac{1}{n}(V_{SCCM} + \Delta v_{SCCM}) \tag{3.12}$$

where V_{SC} is the voltage across the supercapacitor string, Δv_{SC} corresponds with the energy exchange on the supercapacitor string during buck and boost operation mode of the half-bridge, resulted from performing EIS testing.

Therefore, the amount of energy stored in a supercapacitor string can be rewritten as:

$$E_{SC} = \frac{1}{2} C_{SC} V_{SC}^2 \tag{3.13}$$

After substituting (3.13) into (3.14), the energy stored in SCCM is written as:

$$E_{SCCM} = \frac{1}{2n^2} C_{SC}(V_{SCCM}^2 + \Delta v_{SCCM}^2 + 2V_{SCCM}\Delta v_{SCCM}) \tag{3.15}$$

After rearranging (3.15), the energy stored in the supercapacitor string is:

$$E_{SCCM} = \frac{1}{2n^2} C_{SC} V_{SCCM}^2 + \frac{1}{2n^2} C_{SC} \Delta v_{SCCM}^2 + \frac{1}{n^2} C_{SC} V_{SCCM} \Delta v_{SCCM} \tag{3.16}$$

where the energy transfer resulted from the ac signal in the form of P_{ac} is derived as:

$$E_{ac} = \frac{1}{2n^2} C_{SC} \Delta v_{SCCM}^2 + \frac{1}{n^2} C_{SC} V_{SCCM} \Delta v_{SCCM} \tag{3.17}$$

where the $V_{SC\ string}$ consists of dc level and the ripple components resulted from EIS, V_{SCCM} and Δv_{SCCM}.

The ripple energy induced by ac power at the input side is

$$E_{ac} = \frac{1}{2n^2} C_{SC} \Delta v_{SCCM\ string}^2 + \frac{1}{n^2} C_{SC} V_{SCCM} \Delta v_{SCCM} \tag{3.18}$$

The instantaneous energy balance between the ripple power from EIS and ripple energy of the supercapacitor string transferred back and forth via the bidirectional SCC as an interface can be written as:

$$\int P_{ripple} dt = \frac{1}{2n^2} C_{SC} \Delta v_{SCCM}^2 + \frac{1}{n^2} C_{SC} V_{SCCM} \Delta vc_{SCCM} \tag{3.19}$$

By taking a few steps towards solving (3.19) for Δv_{SCCM}, the formula can be rearranged as:

$$\Delta v_{SCCM} = -V_{SCCM} + \sqrt{V_{SCCM}^2 + \frac{2|P_{ripple}|}{n^2 C_{SC} \omega} (1 - \cos(\omega t))} \tag{3.20}$$

where C_{SC} corresponds with the total capacitance of the supercapacitor string connected to the lower side of the SCC as input with appropriate voltage rating to withstand the voltage peak with oscillation resulting from EIS excitation which is calculated in (3.20).

The magnitude of this oscillation can be calculated as:

$$|\Delta V_{SCCM}| = -V_{SCCM} + \sqrt{V_{SCCM}^2 + \frac{4|P_{ripple}|}{n^2 C \omega}} = V_{SCCM} + \sqrt{V_{SCCM}^2 + \frac{4(0.1 P_{dc})}{n^2 C_{SC} \omega}} \tag{3.21}$$

The calculated $|\Delta V_{SCCM}|$ is proportional to P_{ripple}, therefore, to find the minimum required total supercapacitor string capacitance and the number of supercapacitors connected in series at the low side of the SCC to maintain the voltage $|\Delta V_{SCCM}|$ within the

acceptable range, the maximum power magnitude of the ac power is required. The maximum $|P_{ripple}|$ is obtained when Z_m is equal to zero, however, this is not the case in practice for FC stacks. The other factor in the model is given, the minimum value of Z_m corresponds to the maximum $|P_{ac}|$. As the largest oscillations appear at low frequency (1Hz), the capacitance effect of the internal impedance is ignored and Z_m is approximated with the polarization resistance of the FC stack. Through diagnosis, the conditions such as degradation, flooding, and drying in FC stack result in an increase of Z_m, leading to a decrease in efficiency of the FC stacks which the value for Z_m can be approximated when starting the FC stack. This value is usually stated in the datasheet of the fuel cell or can be found through testing at the initialization phase of the FC stack.

The system has power losses associating with Z_m (when $Z_m \neq 0$), I_{fc}, and P_{ac} which are usually much lower than the output power $P_{losses} \ll P_{OUTPUT}$, therefore losses can be neglected from (3.21) and be rewritten as:

$$|\Delta V_{SCCM}| = -V_{SCCM} + \sqrt{V_{SCCM}^2 + \frac{0.4P_{dc}}{n^2 C_{SC}\omega}} \tag{3.22}$$

Equation (3.22) defines the highest boundary of oscillation magnitude. The SCCM energy buffer is rated within the obtained electrical rating ($|\Delta V_{SCCM}| + V_{SCCM}$) with the given capacitor of the SC string when applying the ac perturbation at the lowest frequency and at highest P_{ripple}. An example is provided in Figure 3-3 for visualization and demonstrating the impact of energy exchange associated with EIS frequency and the total capacitance of the supercapacitor string.

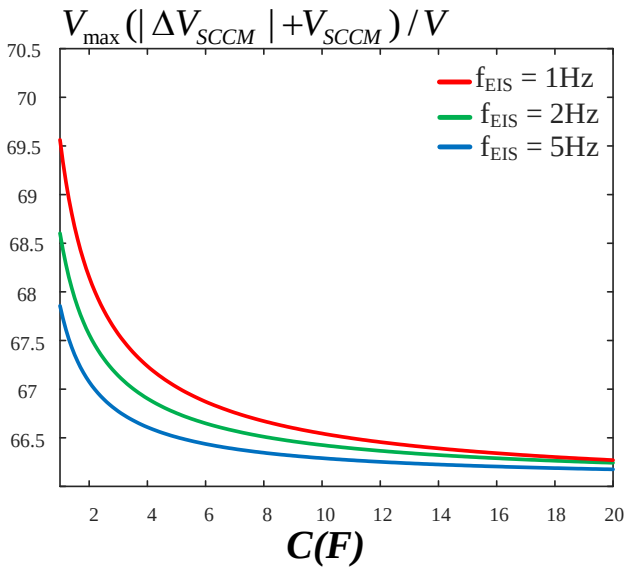

Figure 3-3 Voltage swing vs. SC total capacitance

Referring to (3.22) there are 4 factors which contribute to the voltage swing across the SCCM. The first factor n is the conversion ratio of the SCC. Also, the V_{SCCM} which is associating with the pre-charged voltage of supercapacitor string (V_{SC}). The DC operating point of the FC stack is another factor which is in direct relationship with the amount of energy being transferred during performing EIS testing. And the EIS frequency which has an inverse impact on the voltage swing observed across the SCCM.

3.5. Supercapacitor String Voltage Constraint

There is an important consideration focused on the supercapacitor string located at the low side of the SCC when designing the SCCM. The supercapacitor string has to be pre-charged to certain voltage level to be able to absorb the oscillations resulting from performing EIS testing. In other words, the supercapacitor string which consists of a number of series-connected supercapacitors must not exceed the rated voltage of the string. This consideration provides us with a guideline to determine a window for pre-charging the supercapacitor string connected to the low side of the SCC.

$$V_{SCCM\,max} > V_{SCCM} + \Delta v_{SCCM} \tag{3.23}$$

$$V_{SC\,max} > V_{SC} + \Delta v_{SC} \tag{3.24}$$

where $V_{SC\,max}$ is the maximum allowable voltage across the supercapacitor string connected to the low side of the SCC, V_{SC} is the pre-charged voltage across the supercapacitor string, and Δv_{SC} is the voltage swing across the supercapacitor string. To find out the value for V_{SC} we can use the provided formula in (3.23).

$$V_{SC\,max} = n \times V_{Supercapacitor\ String} \tag{3.25}$$

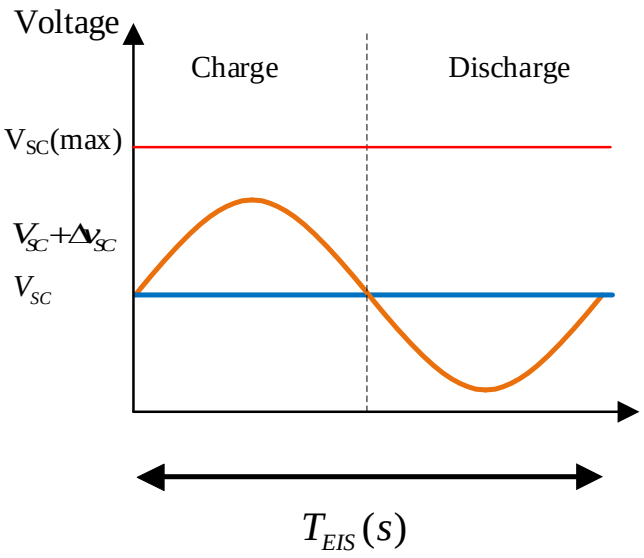

Figure 3-4 Supercapacitor allowable rated voltage constraint

3.6. Switched-Capacitor Converter Optimal Conversion Ratio

The operating principles of the SCCs are discussed in Chapter 2, where a cascaded high step-up bidirectional SCC is chosen over the other existing SCC topologies for this project. As depicted in Figure 3-5, the low side of the converter is where the supercapacitors are connected. Here, the determination of optimal conversion ratio is discussed and reasonings are presented. Referring to Figure 3-1, the placement of the SCCM energy buffer is identified and the requirement for reaching the minimum voltage from the SCC which correlates with the rated power of the fuel cell is discussed here.

The cascaded SCC proposed in [28] can achieve any integer number for conversion ratio by cascading SCCs. Here, a 1:9 cascaded SCC in Figure 3-5 is proposed for SCCM design to meet the requirement of NEXA 1.2kW FC stack to better explain the concept. Considering the constraints of this application mentioned in Chapter 2, one of the limitations considered in determining the optimal conversion ratio for the cascaded SCC is to have a large number of cascaded converters to reach a high conversion ratio, which decreases the obtainable conversion ratio in practice as stated in [27] and results in a large end design of the system. Also, adding multiple stages to the SCC results in increasing the total device power rating (TDPR) of the system [28], which is not favorable if not needed due to the increase of complexity, the chance of component failure, cost, operation limitation (e.g. efficiency drop, conversion ratio drop .etc.), and size of the SCC as the main drawback for this design. A more detailed analysis for choosing the conversion ratio 1:9 is presented in Chapter 4.

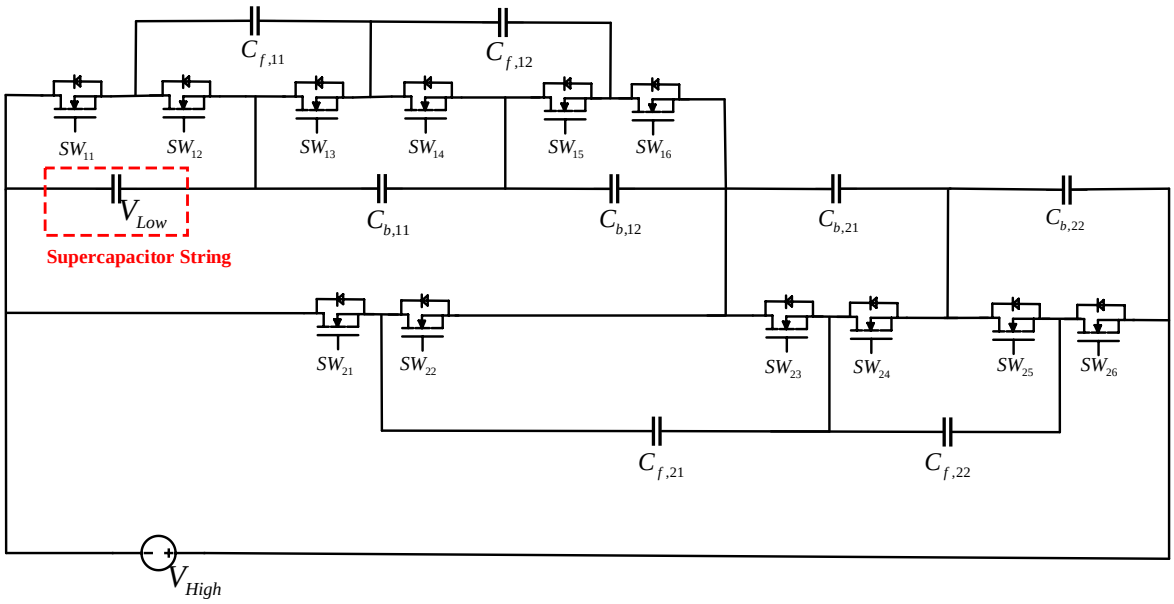

Figure 3-5 Cascaded Switched-Capacitor Converter 1:9 conversion ratio

The selected fuel cell to demonstrate the design is a NEXA 1.2kW with a voltage rating of 36-42 volts where the V_{SCCM} is the minimum voltage rating for the SCC module and should be above V_{fc} in contemplation of functioning appropriately. In order to make a comparison to find the optimal conversion ratio for this application while satisfying the application constraints explained in Chapter 1, the details of four conversion ratios are described as well as the approximation of the required capacitance and the number of series-connected supercapacitors to provide the guideline design for the SCCM.

To determine the pre-charged voltage of the supercapacitors connected in series on the low side of the SC converter and the minimum required voltage of V_{SCCM} connected to the half-bridge for the buck-boost operation which is correlating with maximum voltage from the fuel cell side (V_{fc}), the relationship can be expressed as in (3.21). Here V_{SCCM} is the voltage determined in (3.22) to provide the voltage support for the converter to perform EIS and absorb the resulted oscillations from EIS generating process. The pre-charged stage is done with consideration of the required capacitor for the energy exchange rate explained in the following section of this chapter. n is the number of supercapacitors connected in series to achieve the minimum required voltage for the SCCM energy buffer output terminals connected to the auxiliary EIS converter. Commercially available supercapacitors voltage rating varies from 2~3V, although the most commonly used supercapacitors are with 2.7V rated voltage, therefore, 2.7V is substituted in (3.27) for calculating the supercapacitor string voltage and leading to the realization of the number of supercapacitors required in series.

$$V_{SCCM} = Conversion\ Ratio\ \times V_{Supercapacitor\ String} \tag{3.26}$$

$$V_{Supercapacitor\ String} = n\ \times\ V_{Supercapacitor\ Rated\ Voltage} \tag{3.27}$$

$$V_{SCCM} = n\ \times V_{Supercapacitor\ String} \tag{3.28}$$

where n is the number of series-connected supercapacitors, and V_{SCCM} the voltage across the SCCM energy buffer terminals.

An index which can be used as an indicator to estimate the size of SCCs is to calculate their TDPR value. This value is obtained through the summation of the voltage rating on all capacitors and switches.

$$TDPR_{SCCM} = \sum_1^x C_{bx} + \sum_1^x C_{fx} + \sum_1^x SW_x \tag{3.29}$$

This value can be regarded as a separate number for the entire component on the SCC or individually calculated for each component type. For this part, 3 conversion ratios are presented to demonstrate the impact of conversion ratio increase on the size of the SCC. Also, for better visualization, a radar graph Figure 3-6 is provided here, depicted for each component on the SCC.

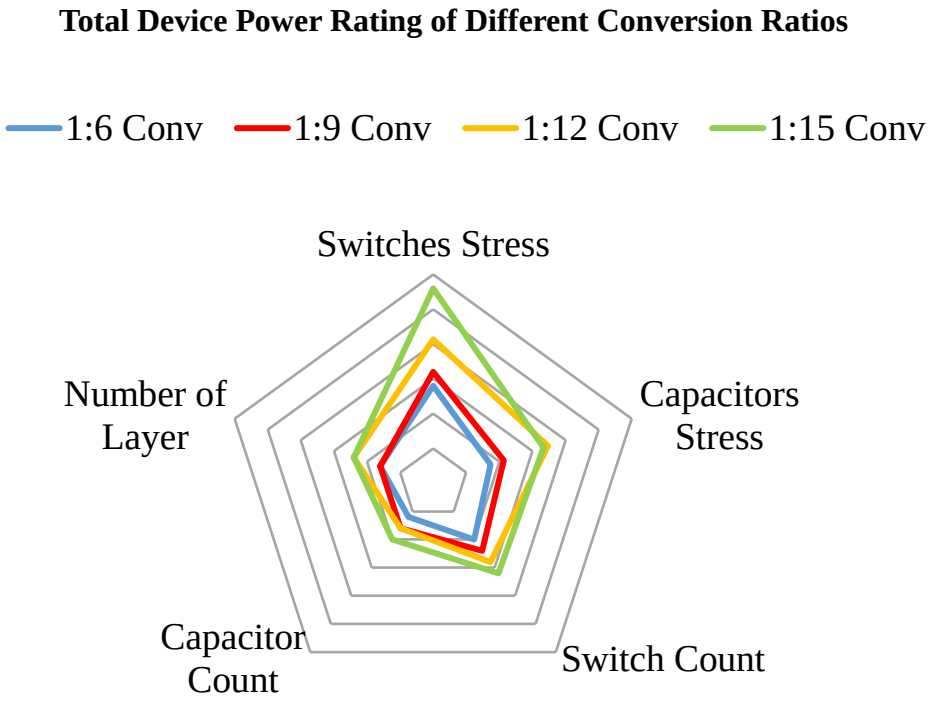

Figure 3-6 TDPR Radar Graph for Different Conversion Ratios

To provide a general description about the information accessible from the radar graph, as the voltage stress or the number of components increases, the radar graph expands

and gets closer to the outer layer, whereas this is the opposite when the abovementioned values are smaller.

3.7. Energy Exchange

The limitation on the latent layer of SCC imposed by the ac signal EIS perturbation generation due to the energy exchange is explained and analyzed here in this section. Output capacitors and bypass capacitors may be used interchangeably.

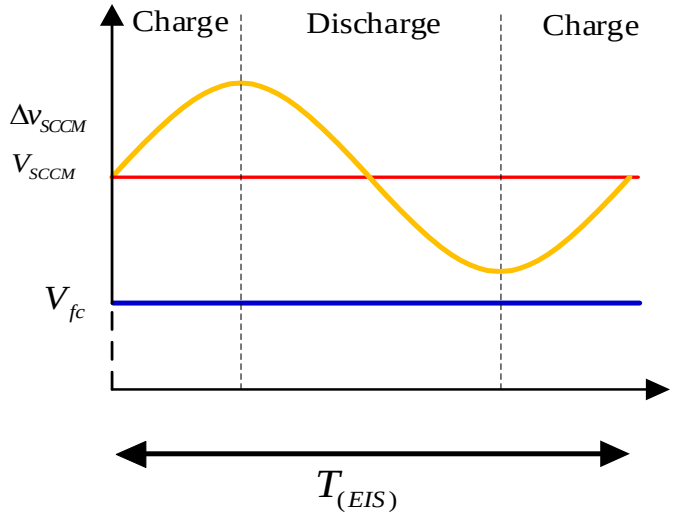

Figure 3-7 Energy exchange

$$E = \int_0^t P(t)dt \tag{3.30}$$

The energy exchange between the supercapacitor string and the ac signal perturbation generated by EIS is shown in Figure 3-7.

As shown in Figure 3-8 and formulated (3.22), the magnitude of the ripple imposed on the supercapacitor string via the SCC is correlating to the half-bridge converter operating values and EIS frequency. The provided waveform for the switched capacitor in [44] is used towards combining the switching frequency of the SCC and the EIS frequency depicted in Figure 3-8. All the components of the SCC are selected following the maximum voltage connecting on the terminal voltage the supercapacitor string to withstand the

voltage variation, as a result, the maximum $|P_{ripple}|$ needs to be found to determine the maximum voltage stress on switches and ceramic capacitors of the SCCM. Therefore, the generalized formula for energy exchange between supercapacitor string through SCC can be written as:

$$E_{charge/discharge} = \sum_{1}^{m} \frac{E_m}{m} \tag{3.31}$$

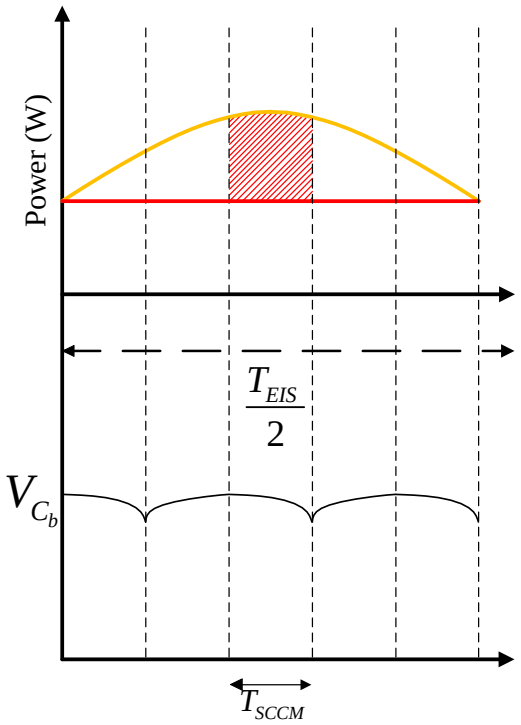

Figure 3-8 SCCM switching waveform and EIS signal

where the amount of energy being transferred decreases as the ac perturbation frequency (represented by m) of EIS increases, therefore, the largest oscillations appear at low frequencies.

By neglecting the energy losses of the system, the energy transfer during charge and discharge can be written as:

$$E_{transfer} = E_{charge} - E_{discharge} \tag{3.32}$$

As the ac perturbation is composed with a sine wave, therefore, it can be concluded that the charge transferred during charge and discharge is symmetrical and of the same value. Therefore, energy transfer is written as ($E_{total} = 0$):

$$E_{total} = E_{charge} - E_{discharge} \tag{3.33}$$

$$0 = \sum_1^m \frac{E_m}{2m} - \sum_1^m \frac{E_m}{2m} \tag{3.34}$$

To be able to absorb the ac signal resulted from EIS and provide the required energy for boost operation, the assumption made previously should be true.

$$E_{SCCM} > E_{charge}\ or\ E_{discharge} \tag{3.35}$$

The higher the frequency of the EIS excitation, the faster and more instantaneous the energy demand provided from the SCCM energy buffer becomes.

3.8. EIS Load Profile

As it is previously explained, the output power of the FC stack is in a relationship with the internal resistance of the stack, which varies and grows bigger as the FC stack ages. On the other hand, the maximum power exchanged during performing the EIS testing is when this internal resistance is zero (although cannot be the case in practice). Therefore, by knowing the voltage across the SCCM terminals and the internal resistance, the EIS load is depicted in Figure 3-10.

Figure 3-9 Load profile for NEXA 1.2kW

Deriving the load profile of the EIS auxiliary converter provides us with the required information such as discharge current which is crucial for sizing the auxiliary EIS converter. As shown in Figure 3-10 the peak power here is approximated, specifying the window of the load demand from the SCCM.

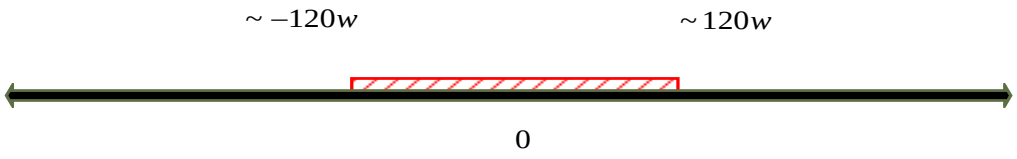

Figure 3-10 Power profile for NEXA 1.2kW

This graph provides the knowledge of the maximum power stated in (3.9), from which the discharge current can be derived.

3.9. Switched-Capacitor Converter Probable Limitations

As previously mentioned, one of the limitations is related to performing the EIS ac signal perturbation with low frequency, whereas, in this section, the correlation between the ac perturbation frequency and the output capacitors of SCC is investigated. In general, it can be perceived from the significant difference between the SCC switching frequency and EIS frequency, there might be no limitation when $SCC_{F_{SW}} \gg EIS_{freq}$. Although, in some cases, the presumption made above may not apply. When generating ac perturbation signals with high frequency, the latent layer of the cascaded SCC should be sized and have enough energy stored to avoid the depth-of-discharge (DoD) rate reaching the level that the discharge rate is higher than the charge shuttling rate which ultimately leads to a distorted EIS signal as there is not enough energy to be supplied to the half-bridge for generating EIS signal.

$$E_{SCC\ Output\ capacitors} \gg E_{EIS\ discharge} \tag{3.36}$$

Energy stored in the output capacitor of the SCC is calculated through:

$$E_{Output\ Capacitor} = \frac{1}{2} C_{total} V^2_{Output\ capacitors} \tag{3.37}$$

Chapter 4.

Case Study and Design Consideration

In this chapter, the commercially available fuel cell NEXA 1.2kW developed by Ballard Power System is used for a case study to examine the functionality of the proposed energy buffer SCCM with auxiliary EIS converter. This FC stack is rated for 1.2 kW with 36-42 V at its terminals. As explained in Chapter 3, the voltage of the SCCM needs to be higher than the terminal voltage of the FC stack for the auxiliary EIS converter to function properly. The chosen low side voltage for the SCCM energy buffer is compared in Table 4-1. The number of supercapacitors connected in series is in direct relationship with the required SCC conversion ratio. Therefore, the trade off between the conversion ratio which correlates with the number of components and the TDPR of the whole SCC is considered for this design analysis.

To revisit the requirement of this application, having a compact sized SCC as a bidirectional interface is one of the main factors. By choosing the logical and sensible conversion ratio, we can reduce the cost and size of the converter. Therefore, a general comparison is being done for different components on the SCC using TDPR as an indicator of this comparison. A radar graph is shown in Figure 3-6 for better visualization for this evaluation.

Here, based on the data provided in Table 4-1, the correlation between the number of series-connected supercapacitors can be derived. As explained in Chapter 3, the number of series-connected supercapacitors and the supercapacitor string pre-charged voltage value reflects on the high side of the SCCM energy buffer. There are potential problems for a large string of supercapacitors connected in series. Cell imbalance is one of the considerations; also, capacitance variation due to the manufacturing tolerances can decrease the total capacitance of the supercapacitor string, resulting in the SCCM not being able to provide the required voltage support to the auxiliary EIS converter. Therefore, it is desirable to avoid a large string of series-connected supercapacitors. For a conversion ratio of 1:6, the number of the required series-connected supercapacitors is 4, which offers the lowest TDPR value for the SCC, but a larger solution for SCCM as a whole due to the largest required number of series-connected supercapacitors. On the other hand, for a 1:9 conversion ratio, the number of series-connected supercapacitors is 3 and the SCC has a slightly higher TDPR, offering a slightly bigger SCC but a more compact SCCM due to eliminating one supercapacitor in the string. For 1:12, the number of switches and capacitors increases which results in a higher TDPR factor. Also, by increasing the number of switches, the SCC requires a larger number of gate drivers, leading to a bigger design while still needing 3 series-connected supercapacitors in the low side of the SCC. In the end, for a 1:15 conversion ratio, there is a need for two series-connected supercapacitors which is one supercapacitor less than 1:9 and 1:12 conversion ratios but resulting in a significantly higher TDPR.

Therefore, after analyzing the information explained above, 1:9 offers the best conversion ratio for the SCC which works as a bidirectional interface between the supercapacitor string and the auxiliary EIS converter.

In Table 4-1, the TDPR and the number of series-connected supercapacitors are presented. As the number of stages on cascaded SCC is also deterministic, this value is also stated in the table to help with the comparison.

Table 4-1 SCC with different conversion ratios

Conversion Ratio	Number of supercapacitors	Number of Stages	TDPR Capacitor	TDPR Switch
***n* 1:6**	4	2	2L+4H	4L+6H
***n* 1:9**	3	2	4L+4H	6L+6H
***n* 1:12**	3	3	2L+4M+2L	4M+6M+4M
***n* 1:15**	2	3	4L+2M+4H	6L+4M+6H

Voltage rating for capacitors and switches are grouped into L: lower voltage rating, M: medium voltage rating, and H: high voltage rating

4.1. EIS Load Profile for NEXA 1.2kW

The load profile for the auxiliary EIS converter power demand depicted in Figure 4-1 is needed to determine the discharge current of the SCC which is required for determining the switching frequency and the required capacitance of bypass and flying capacitors when designing the SCC. The auxiliary EIS converter works as a reactive power generator by controlling the magnitude of the generated current. This process mimics the effect of a variable load connected to the SCCM. The auxiliary converter should be capable of handling 10% of the power rating of the FC stack referring to formula (3.1) provided previously in Chapter 3. Therefore, by knowing the terminal voltage and the power rating of the half-bridge auxiliary EIS converter, we can obtain the load and profile of the auxiliary converter. The power rating of the NEXA (1.2 kW) is used for deriving the load profile depicted in Figure 4-1.

$$P_{Aux\ EIS\ max} = I_{discharge} \times V_{fc} \tag{4.1}$$

where $P_{Aux\ EIS\ max}$ is the peak power for the auxiliary EIS converter which is observed when the Z_m internal resistance of the FC stack is assumed to be zero. V_{fc} is related to the DC operating point of the FC stack and substantially, $i_{discharge}$ is derived to help us towards finding the load profile depicted in Figure 4-1 of the auxiliary EIS converter.

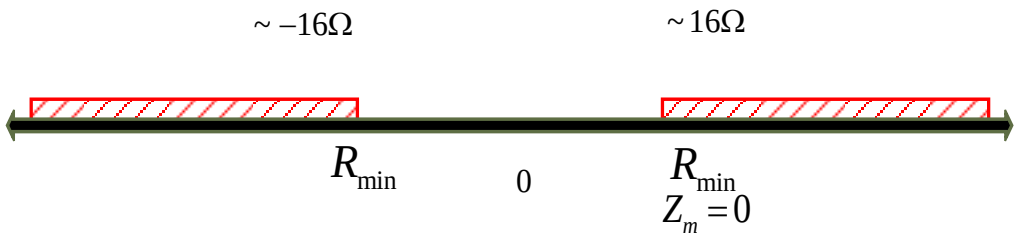

Figure 4-1 Load profile for NEXA 1.2kW

4.2. General Overview of the Power Losses of the SCC

Although the power losses of the system is disregarded referring to the proven fact that SCC is known to be a very energy-efficient converter and acknowledging the fact that the whole auxiliary EIS system does not operate on regular basis and mostly operates on certain occasions, therefore, there is not much emphasize on the power losses and efficiency of the SCC converter. However, to help us to have a better insight of the dissipated power in the SCC converter employed as the interface, here in Figure 4-2 power losses correlating with different layers of the SCC is depicted. As it can be seen, by increasing the voltage stress on each stage, the need for larger switches leads to higher $R_{DS}(ON)$. Ultimately, higher parasitic resistance of the MOSFET ($R_{DS}(ON)$) will lead to higher dissipated energy. Therefore, as perceived, the losses on the second layer are relatively higher than the losses on the first layer. The parasitic resistance of the chosen ceramic capacitors (R_{ESR}) considering the number of required ceramic capacitors to be connected in series makes the R_{ESR} negligible, therefore, omitted from the analysis below.

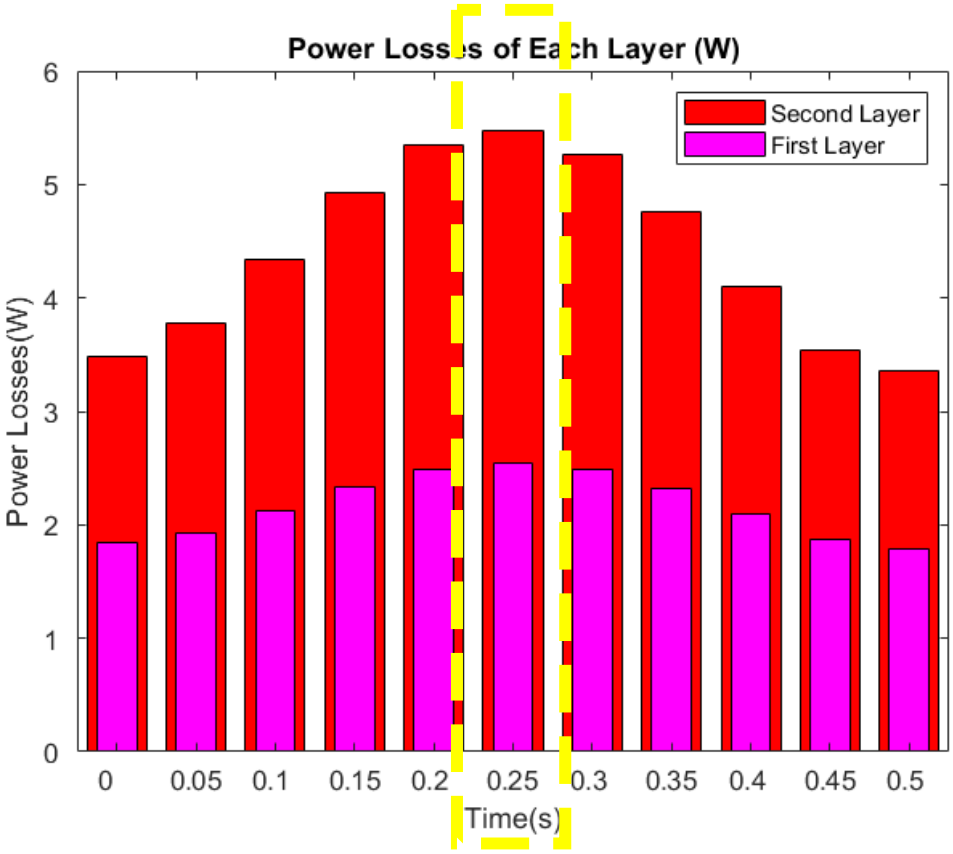

Figure 4-2 Power Losses of Each Layer of SCC

The above analysis and demonstration also support the assumption made before to possibly avoid cascading multiple SCCs together as the losses grow dramatically when adding layers. The efficiency of the SCC is calculated as (3.21):

$$\eta_{SCC} = V_{OUT} - V_{In} \tag{4.2}$$

With respect to (3.21), the calculated efficiency in the dotted area shown in Figure 4-2 is calculated to be η_{SCC} >93%.

4.3. Supercapacitor String Capacitance

The terminal voltage of the proposed SCCM should be above the V_{fc} determined by the rated voltage of the FC stack. This condition is required for the SCCM to be able to provide the required voltage support to the auxiliary EIS converter for generating the ac perturbation signals with respect to the necessary condition of $V_{SCCM} > V_{fc}$. Therefore, the capacitance of the supercapacitors should be sized appropriately to be able to absorb the oscillations resulting from EIS excitation.

$$|\Delta V_{SCCM}| = -V_{SCCM} + \sqrt{V_{SCCM}^2 + \frac{0.4P_{dc}}{n^2 C_{SC}\omega}} \tag{4.3}$$

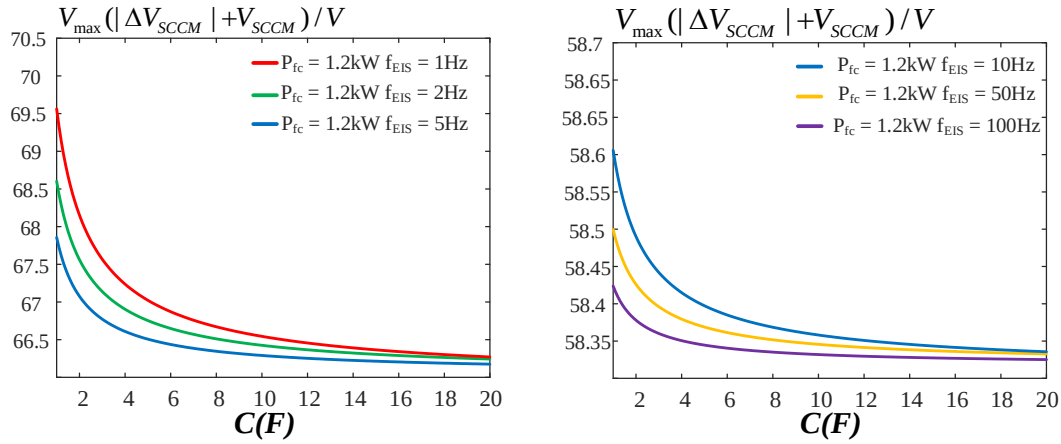

Figure 4-3 Capacitance vs. voltage swing across the SCCM under 1.2kW FCS

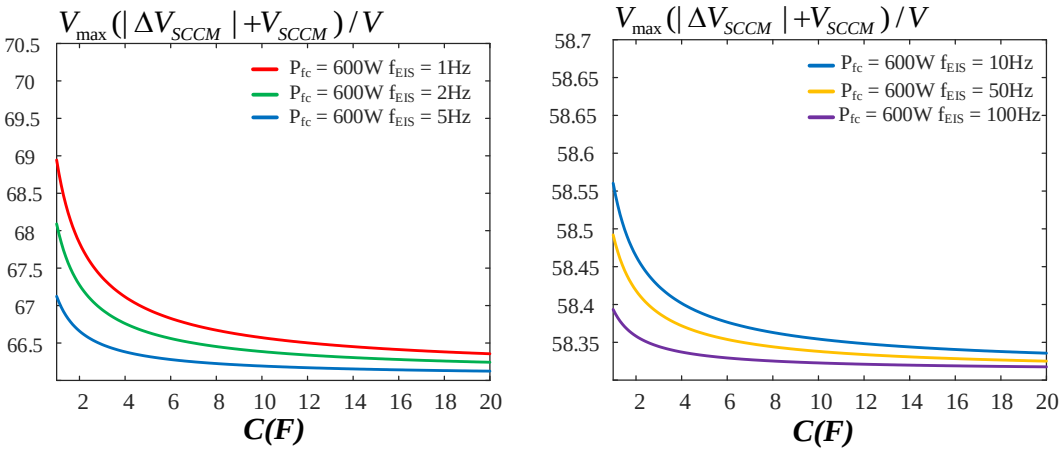

Figure 4-4 Capacitance vs. voltage swing across the SCCM under 600W FCS

By looking at the (4.3), in Figure 4-3 the voltage swing across the V_{SCCM} terminal is depicted considering the DC operating point of FC stack which is NEXA 1.2kW. As it can be seen, by increasing the EIS frequency, the voltage swing becomes smaller and in infinite decays to V_{SCCM} which is the multipilication of the conversion ratio (n) and the V_{SC}, i.e., the pre-charged supercapacitor string voltage. In Figure 4-4, the DC operating point for the FC stack is set as $20A$. The voltage swing which is the reflection of energy being exchanged during charge and discharge of the supercapacitor string is lower than the previous DC operating point, showing the importance of the DC operating point on energy exchange.

4.4. Supercapacitor String Allowable Voltage

As explained in Chapter 3, the number of supercapacitors in series and the conversion ratio of the SCC converter is important to determine the pre-charged voltage of the supercapacitor string. In Figure 4-5 the voltage swing is depicted for 3 series-connected supercapacitors in the low side of the SCC.

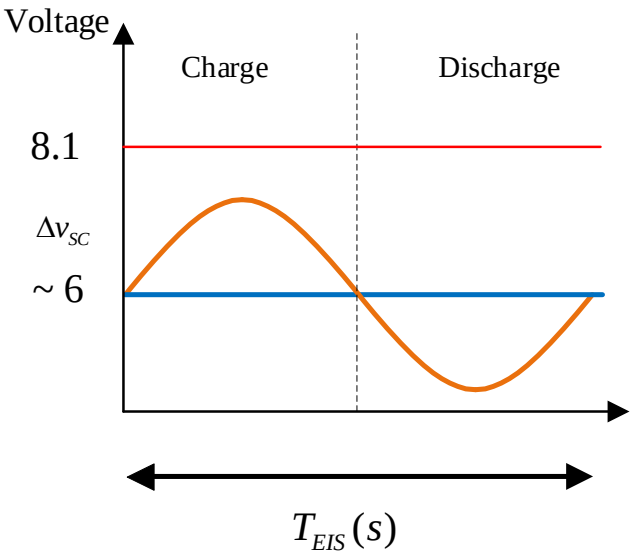

Figure 4-5 Voltage swing across the supercapacitor string resulted by energy exchange

4.5. Parameters Design

As explained in Chapter 2, the determination of the switching frequency and the capacitance for flying capacitors as well as bypass capacitors are the deterministic factors when designing the SCC. Here, with respect to the derived formula, the suitable switching frequency and capacitor capacitance are presented.

$$C_{bypass} = \frac{\Delta t \; i_{discharge}}{k \; V_{bypass}} \tag{4.4}$$

where C_{bypass} is the capacitiance of the bypass capacitors, $i_{discharge}$ is the discharge current associating with the output power load demand, k is the allowable ripple represented in percentage which is derived based on the output power regulation, and V_{bypass} is the voltage across the capacitor.

On the other hand, referring to the abovementioned control strategy with respect to the duty cycle of this SCC control algorithm, determination of capacitance for the flying capacitors is derived as:

$$C_{flying} = \frac{1}{D} \; \frac{\Delta t \; i_{discharge}}{k \; V_{bypass}} \tag{4.5}$$

Table 4-2 Conversion Ratios Comparison

Conversion Ratio	Frequency (f_{SW})	Flying caps Layer#1	Bypass caps Layer#1	Flying caps Layer#1	Bypass caps Layer#1
n 1:9	100kHz	176 μF	88 μF	132 μF	66 μF

The provided waveforms in Figure 3-8 helps us towards the realization of the probable limitations resulted from the EIS testing with high frequency. The voltage ripple of the depth of discharge for the bypass capacitors which are functioning similarly to dc link capacitors are the main cause of the proposed energy buffer failing to provide the required voltage for the auxiliary EIS converter to generate the ac perturbation signals.

4.6. Technology Constraints on SCC Design

When designing the SCC parameters, theoretically derived values may change due to the influence of parasitic elements in a practical system. Stray inductance was observed and considered to change the behavior of the SCC converter for frequencies higher than 100kHz [37]. Also, referring to the fact that there are resistive parasitic factors involved such as the equivalent-series resistance (ESR) for the capacitors and also the power switches which ultimately increase the output impedance of the SCC converter, avoiding the SCC to be able to deliver the required power to the load. Also, the most commonly used gate drives and MOSFETs are only capable of reaching certain switching frequencies depending on the technology chosen for the design, therefore, the parameters chosen in the previous section can be slightly different in practice [50].

4.7. SCCM Different Layers Analysis

Based on the input and output voltage and the number of layers determined by the design of the SCCM energy buffer, the voltage rating can be different. Here in this design, the input voltage for the SCCM is ~6V in the low side and the voltage across the high side of SCCM is ~60V. These values are constantly changing, defined as the voltage swing due to the energy transfer resulting from the oscillations of EIS signals. As explained previously in Chapter 2, the voltage rating on each layer of the SCC is done in accordance to the schematic shown in Figure 3-5.

$$V_{Low} = V_{C_{b,11}} = V_{C_{b,12}} \tag{4.6}$$

$$V_{C_b,21} = V_{C_b,22} = 3V_{Low} \tag{4.7}$$

$$V_{High} = V_{Low} + V_{C_{b,11}} + V_{C_b,12} + V_{C_{b,21}} + V_{C_{b,22}} \tag{4.8}$$

$$V_{High} = 9V_{Low} \tag{4.9}$$

4.8. Components Selection for SCCM

After specifying the design parameters and the voltage stress on each layer, the derived information can serve as guideline for components selections. For the first layer, GRM21BR61D106ME15L ceramic capacitor with rated voltage of 10V is chosen with respect to the assumed pre-charge of the supercapacitor string which is ~ 6V. Respectively, the power switch considered for the first layer is IRFH6200TRPBF with 0.0059Ω (for 10V). The second layer which is product of the $3V_{Low}$ (pre-charge) requires components with higher rated voltage. The ceramic capacitor selected for this layer is GCM32EC71H106KA03L and the power switch is IPZ40N04S5L7R4ATMA1 0.0259Ω (for 40V). As it was mentioned in section 4.3 for finding the suitable total capacitance of the supercapacitor string, here, 3 series connected supercapacitors with part number of TPLH-2R7/4.0WR8X20. The reasoning behind selecting supercapacitors with 4F capacitance is with respect to the capacitance deviation stated in their datasheet which is 20%. Choosing higher capacitance assures the minimum required capacitance is met.

4.9. Simulation and Design Parameters

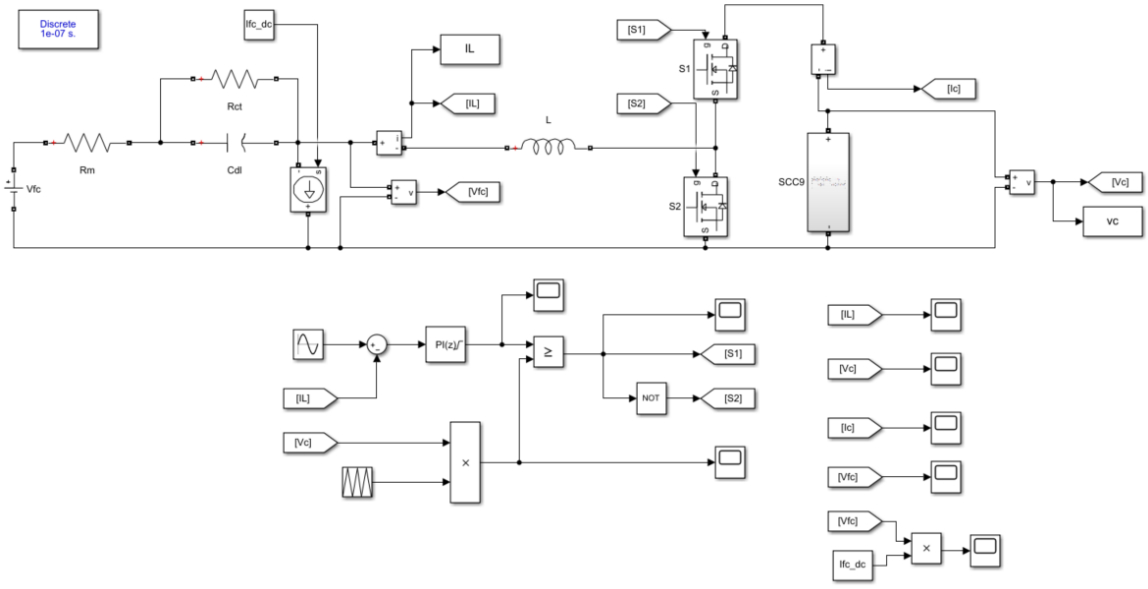

Figure 4-6 Auxiliary EIS conveter conncted to SCCM

A general overview of the auxiliary EIS converter connected with the proposed energy buffer SCCM is shown in Figure 4-6. The newly introduced auxiliary EIS converter is a half bridge assigned to generate the ac perturbation signals. The current is continuously measured and feedback to the system as for performing EIS testing, the generation of current is to be considered, not the voltage.

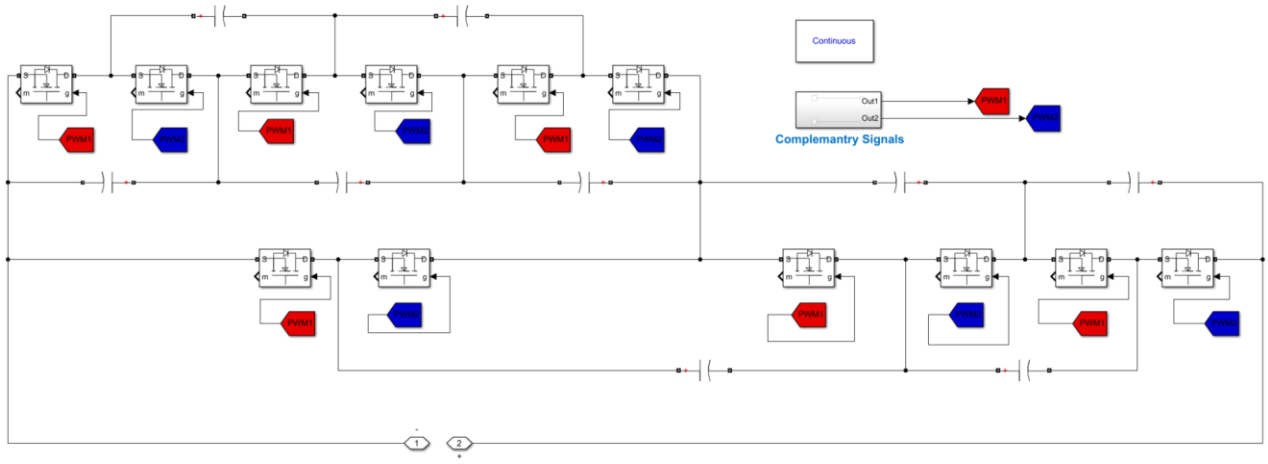

Figure 4-7 Simulation of SCC converter in Matlab Simulink

Here in this section in Figure 4-7, the simulation model used to build the SCC is shown. As it was discussed before, the ESR of the ceramic capacitors are neglected and not used when simulating due to their very small ESR. The switches are orchestrated and controlled with a complementary pair of PWM signal. The gating signals generated with the clock are depicted in red and blue colors for better visualization.

4.10. Simulation Results

The results of the proposed SCCM energy buffer under different EIS frequencies are provided in this section. The optimal conversion ratio is considered to be 1:9 with a requirement of $V_{SC} > 5.6V$ (low side) pre-charged supercapacitor string to meet the requirement for generating the ac perturbation.

In Figure 4-8, Figure 4-9, and Figure 4-10, simulation results are presented for 3 different frequencies of 5 Hz, 50 Hz, and 1000 Hz under 40 A working condition whereas

in Figure 4-13, Figure 4-14, and Figure 4-15 ac perturbations are generated under 20A working condition for FC stack with different frequencies presented, tailored for different conditions of diagnosis. The chosen FC stack as explained before is Ballard NEXA 1.2kW power rating with 36-42V_{FC}. The non-distorted signals prove the full functionality of the SCCM energy buffer module and the capability to work as an energy buffer for this application.

As it was discussed before, due to the probable limitations imposed on the SCCM in EIS testing with higher frequencies, a voltage drop on the terminal voltage of the SCCM was observed, resulted by not choosing the appropriate switching frequency which had led us towards the realization of the abovementioned limitations. Three frequencies 5Hz, 50Hz, and 1000Hz are generated as EIS ac perturbation signals and the energy exchange correlating with Δv_{SCCM} is observed which decreases by increasing the EIS frequency. The lower frequencies result in the larger oscillations occurrence shown in Figure 4-8, Figure 4-11, Figure 4-13 and Figure 4-16 while higher EIS frequencies such as Figure 4-10, Figure 4-12,Figure 4-15, and Figure 4-17 may impose limitations on the SCC if the charge shuttling rate is not chosen with respect to power load demand. As observed, by selecting an appropriate size for output capacitors and SCCM switching frequency, the SCCM is capable of providing appropriate bidirectional energy flow as an interface between the supercapacitor string and EIS auxiliary converter. Also, provided simulation results in Figure 4-9, Figure 4-11, Figure 4-14 are presented to demonstrate the behavior of SCCM energy buffer for moderate frequencies.

Here in Figure 4-8, the frequency of the EIS perturbation signal is set to 5Hz. As can be seen and explained before, the largest oscillations occur during lower frequencies for EIS generation. Also, the voltage swing across the supercapacitor string is wider due to the increase in the amount of the energy being transferred (Δv_{SCCM}).

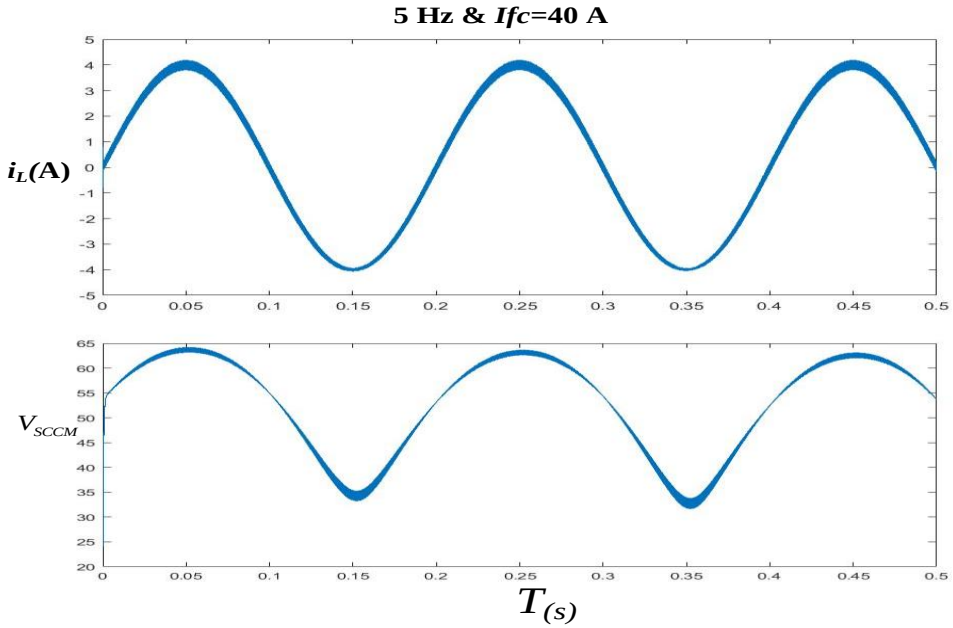

Figure 4-8 SCCM Terminal voltage and EIS i_{ac} perturbation signal in 5Hz

The generated EIS perturbation in this result is with 5 Hz frequency. It is observed that the oscillations are small resulting in larger voltage swing or energy transfer during buck-boost operation modes. The ac signals are successfully generated to perform the EIS testing on the FC stack model which approves the proper functionality of the SCCM module. As mentioned previously, in lower EIS frequencies, larger oscillations are observed.

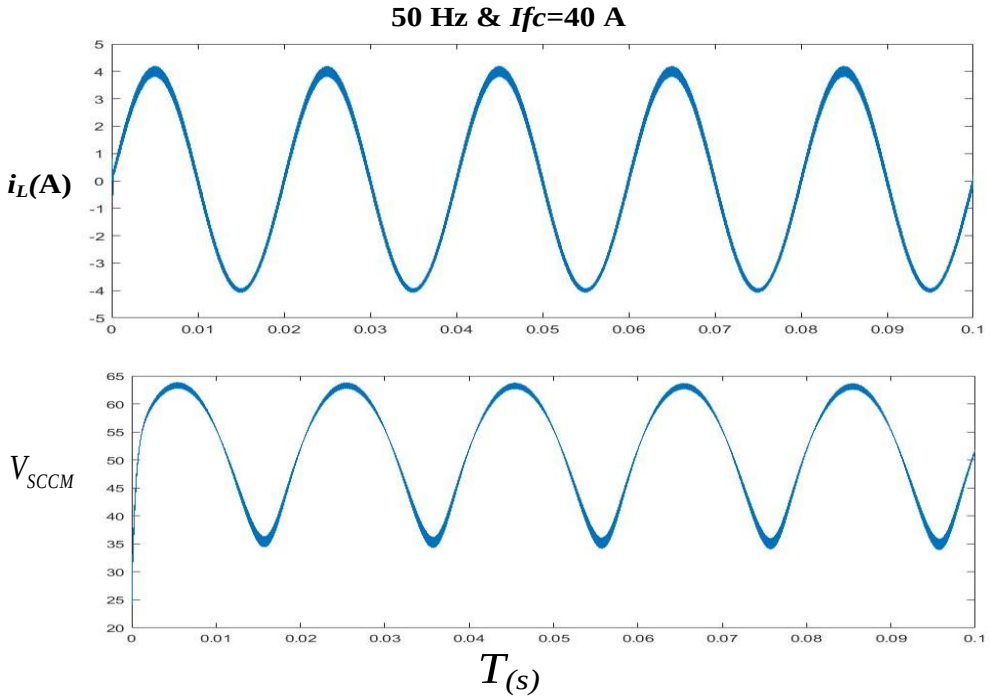

Figure 4-9 SCCM Terminal voltage and EIS i_{ac} perturbation signal in 50Hz

The performed EIS testing with the generated ac perturbation signals in this result is 50 Hz. It is observed that the oscillations are relatively smaller resulting in lower voltage swing or energy transfer during buck-boost operation modes. The ac signals are successfully generated and performed on the FC stack model which approves the proper functionality of the SCCM module in the given EIS frequency.

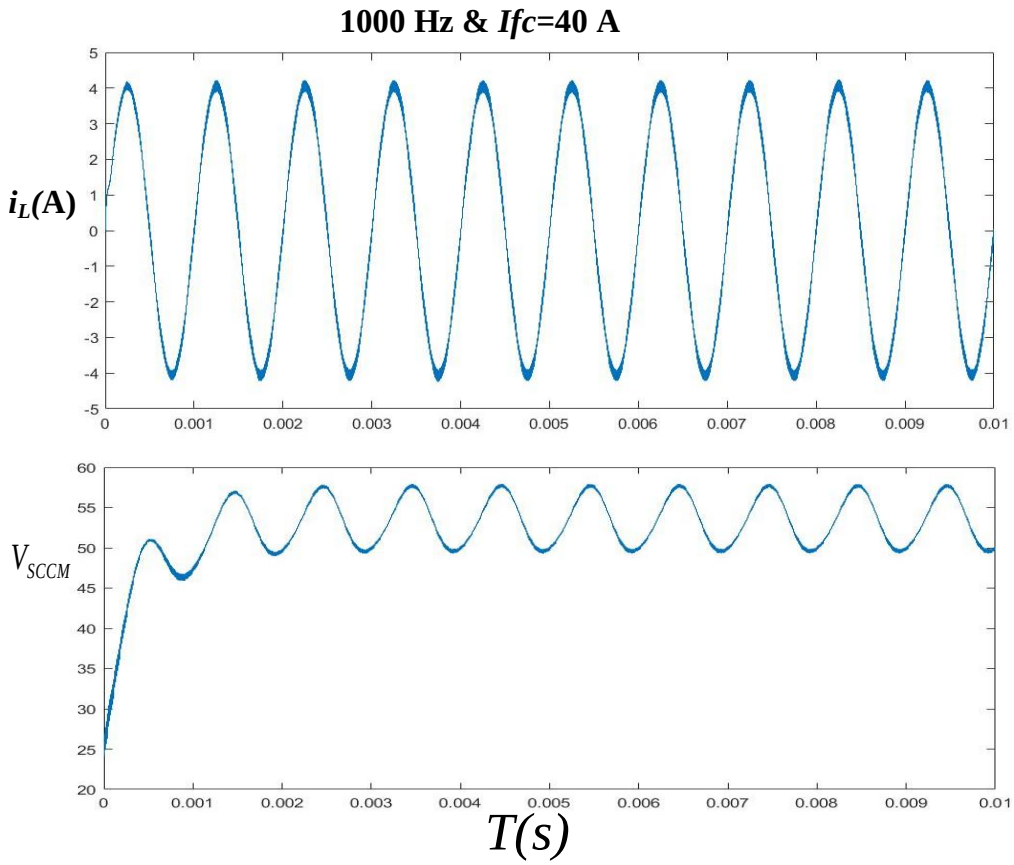

Figure 4-10 SCCM Terminal voltage and EIS i_{ac} perturbation signal in 1000Hz

In comparison to the other two presented results, the results in Figure 4-10 and Figure 4-15 have the lowest oscillations resulting from the energy exchange during the bidirectional operation of the SCCM. The probable limitation related to the switching frequency of the SCCM and the EIS signal is resolved and the signals are properly generated, implying the full functionality of the SCCM.

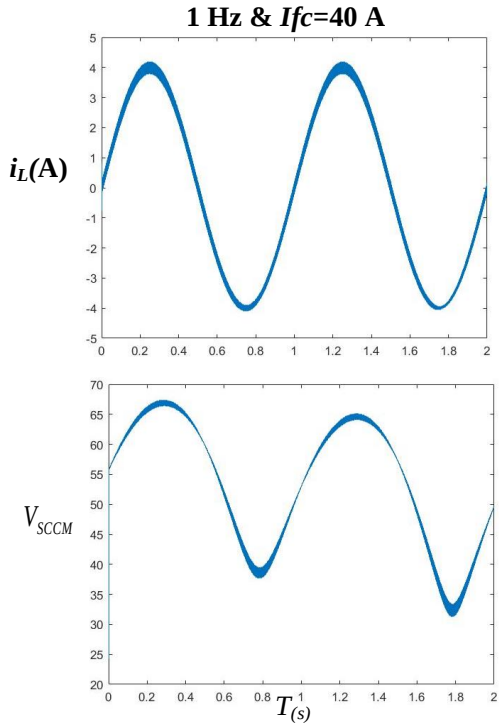

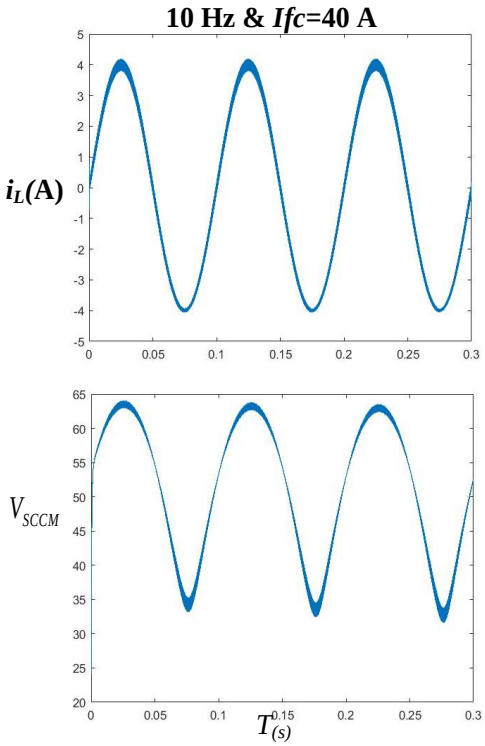

Figure 4-11 (a)EIS signal in 1Hz (b)EIS signal in 10Hz

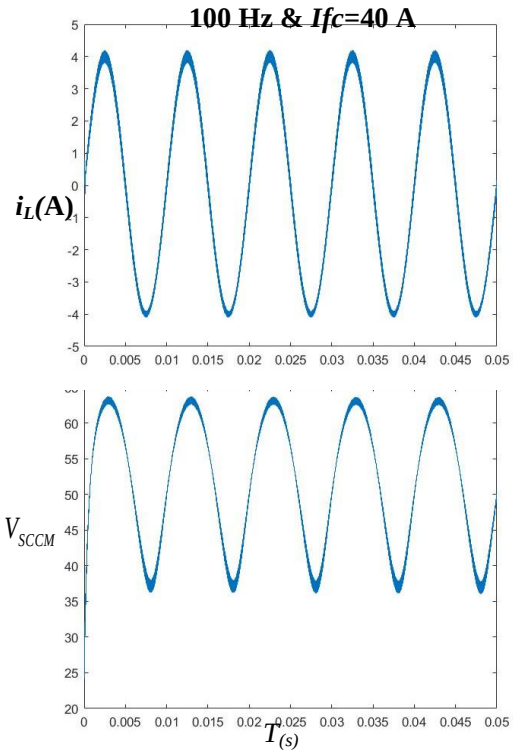

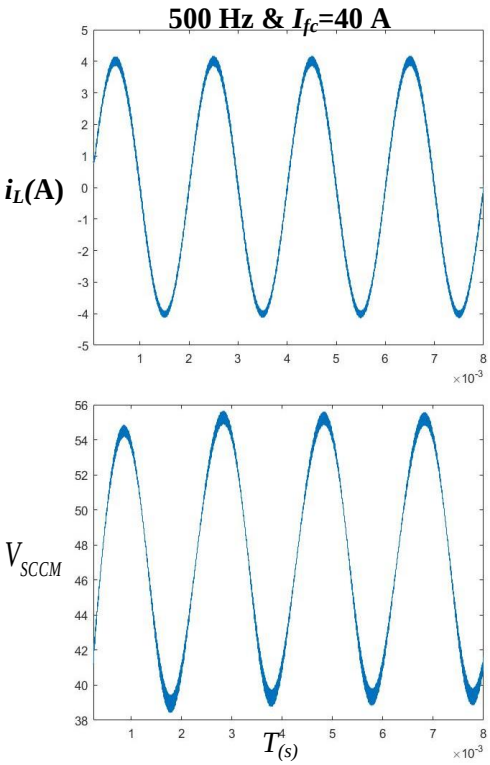

Figure 4-12 (a)EIS signal in 100Hz (b)EIS signal in

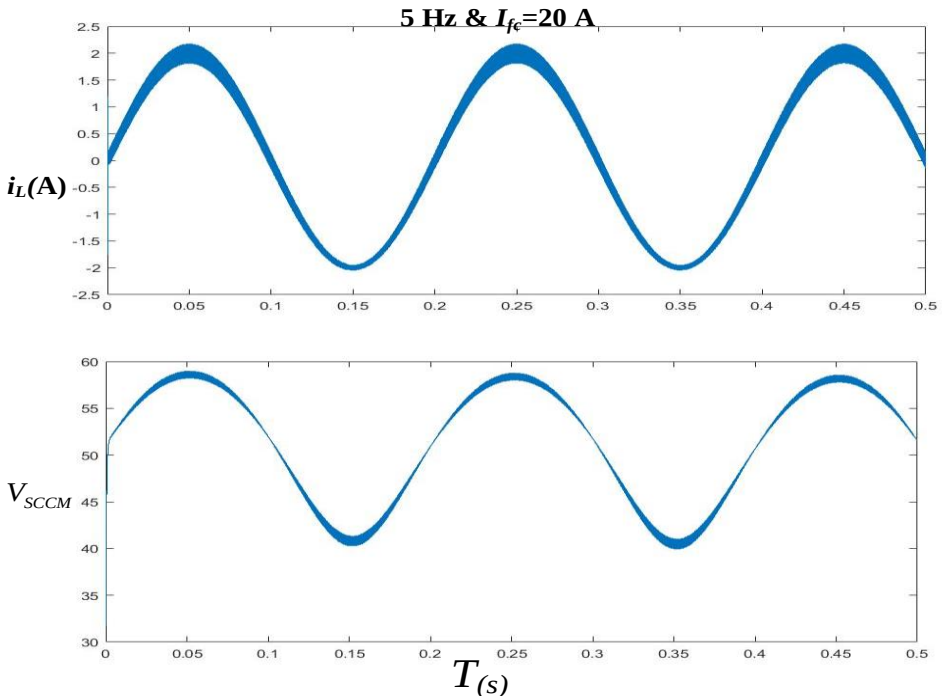

Figure 4-13 SCCM Terminal voltage and EIS i_{ac} perturbation signal in 5Hz

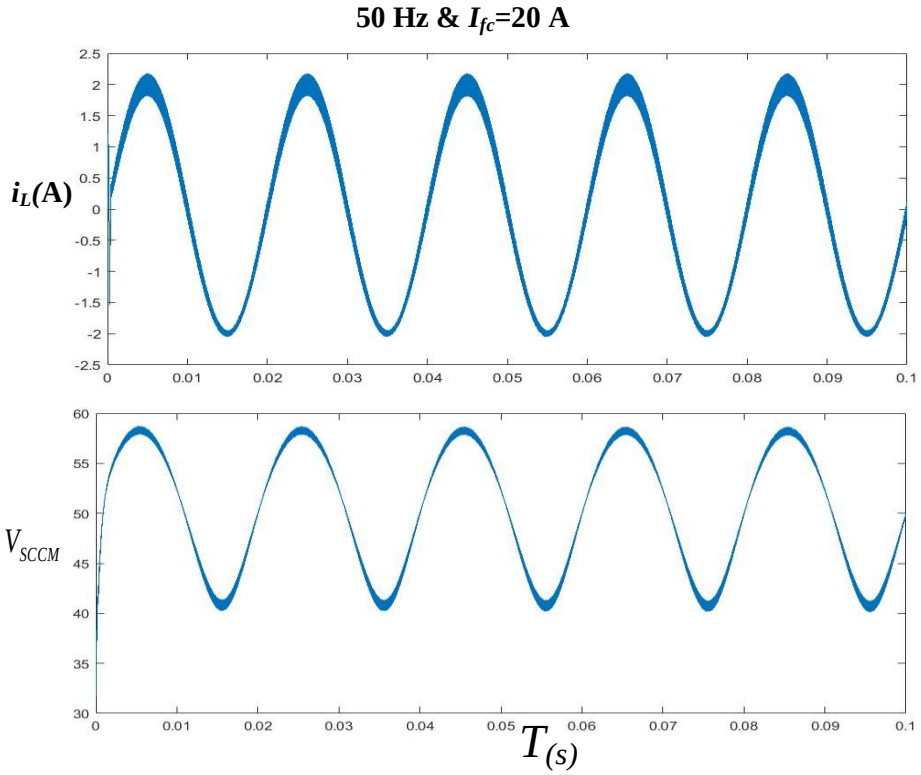

Figure 4-14 SCCM Terminal voltage and EIS i_{ac} perturbation signal in 50Hz

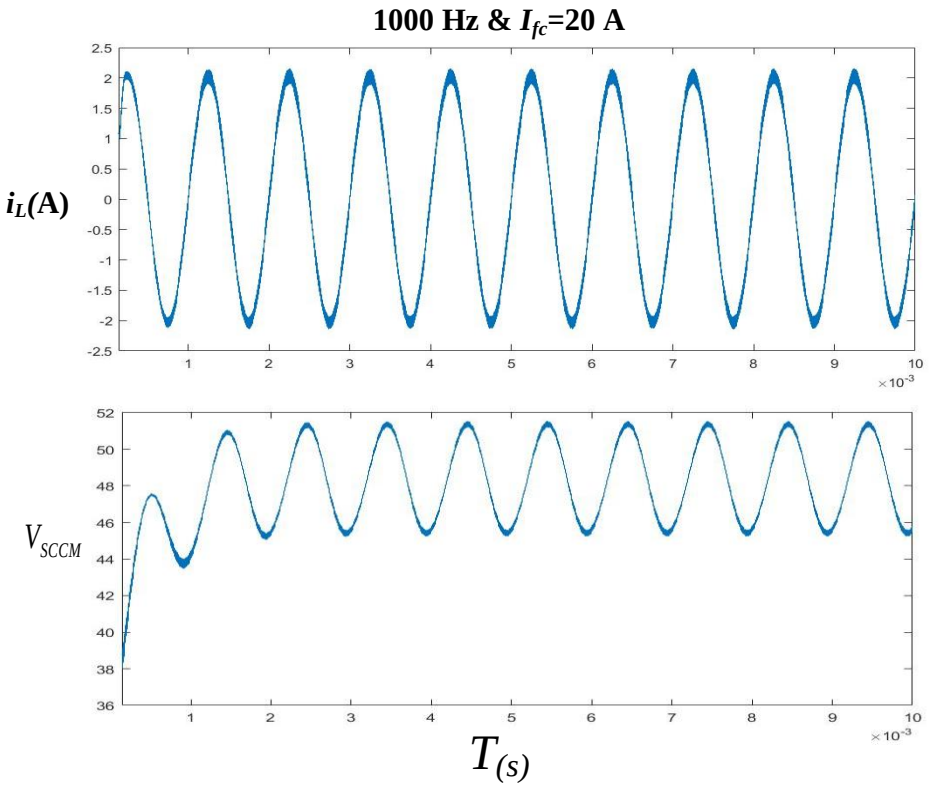

Figure 4-15 SCCM Terminal voltage and EIS i_{ac} perturbation signal in 1000Hz

As it was explained in Chapter 3 and in this chapter in (4.3), with respect to the correlation between the observed oscillations and the EIS testing frequency, the largest oscillations are observable in lower frequencies in the provided results in Figure 4-8 and Figure 4-13. While, the probable limitation which may occur when the charge shuttling rate in the SCC is lower than the discharge rate, reflecting in higher frequencies such as Figure 4-10 and Figure 4-15. As it can be seen, having no distorted ac perturbation signals implies that the SCCM is capable of providing sufficient voltage support for the auxiliary EIS converter to perform EIS testing.

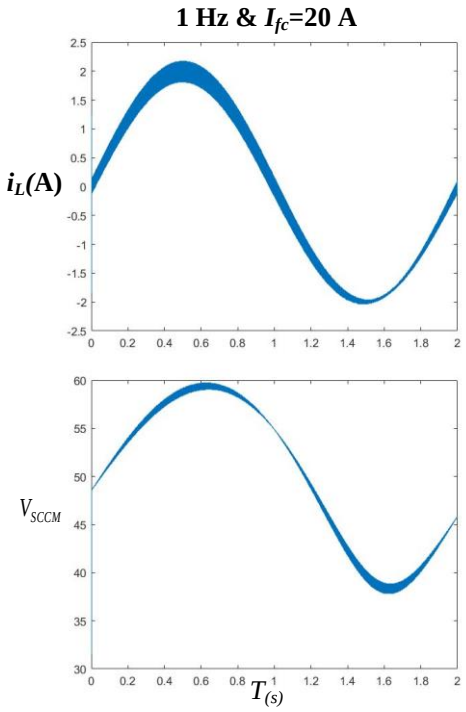

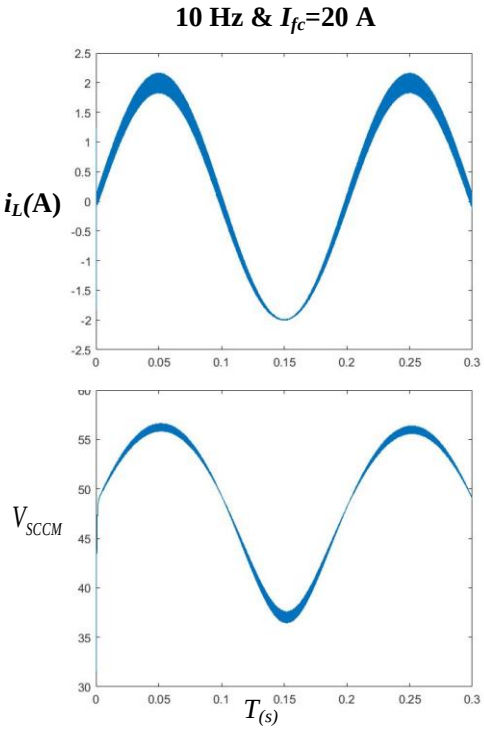

Figure 4-16 (a)EIS signal in 1Hz (b)EIS signal in 10Hz

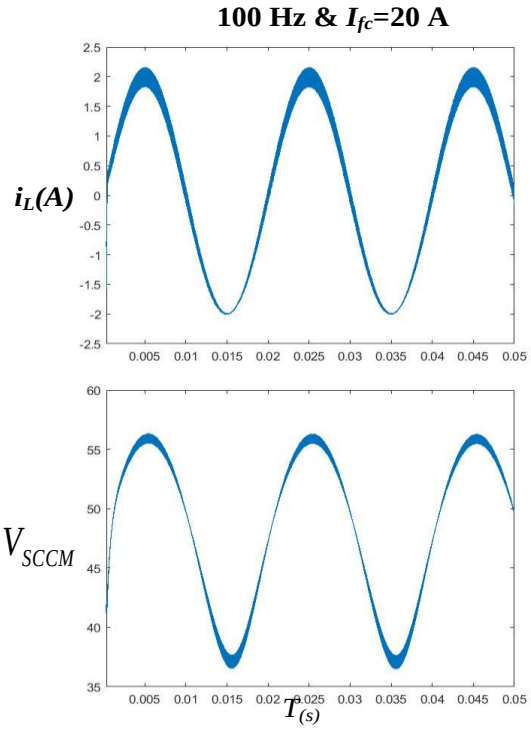

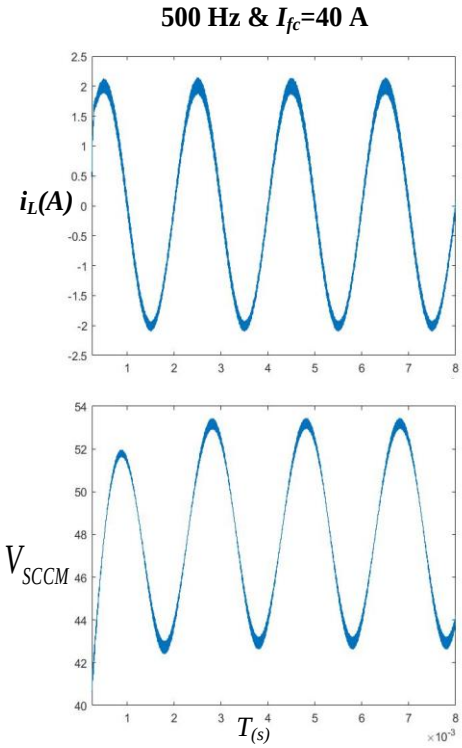

Figure 4-17 (a)EIS signal in 100Hz (b)EIS signal in 500Hz

4.11. Switched-capacitor Limitation Imposed by EIS Frequency

In Figure 4-18 the provided waveform derived from [44] are shown, where the probable limitation imposed by performing EIS testing related to its frequency is demonstrated given the maximum frequency of the performed EIS testing signal is 20 kHz and the switching frequency of the SCC is set to 100 kHz. The discharge period of the EIS frequency is 10 kHz corresponding with the half cycle of its frequency derived from (3.34). The highlighted area under the peak of the EIS frequency in Figure 4-18 is where the maximum power demand occurs. This is for the much higher EIS testing frequencies, where the bypass capacitors should have enough stored energy to provide the instantaneous power required to generate the EIS signal by the auxiliary converter, considering the charge shuttling rate from the flying capacitors. The waveforms in red color shows a depiction of the bypass capacitors being discharged to be higher than the voltage level where the required voltage support for the auxiliary converter is not provided. This phenomenon is basically due to the functionality of the bypass capacitors working similarly to a DC-Link capacitor connected to the half-bridge auxiliary EIS converter. By choosing the correct charge shuttling rate this potential limitation is resolved.

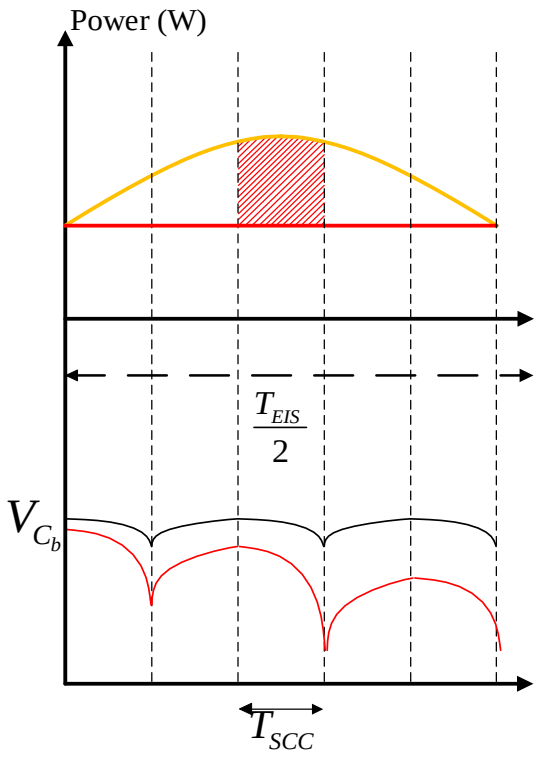

Figure 4-18 SCC waveforms and switching signals - Bypass capacitors during charge/discharge

Chapter 5.

Conclusion

5.1. Thesis Summary

In this thesis, different tools and techniques for diagnostic systems and the necessity of their existence in the FC stack was discussed. EIS diagnostic system working principle and different methods were explained. The advantages of the converter based EIS resulted from its capability of performing online testing were discussed. The newly introduced auxiliary EIS converter to decouple the EIS generating signal device from the main power converter unit was chosen for this study. The benefits and reasoning behind selecting the auxiliary EIS converter to highlight its superiority over other existing solutions was stated and listed. The working principle of the auxiliary EIS converter was explained and the requirement for having an instantaneous energy storage device was addressed.

Different possibilities for instantaneous energy storage devices were stated and the energy buffer consists of a bidirectional high voltage-gain switched-capacitor converter interfaced with a supercapacitor string was proposed. The structure of the proposed energy buffer named SCCM was explained. The working principle of SCCM energy buffer when connected to auxiliary EIS converter was elaborated.

The proposed SCCM energy buffer working principle under the condition of having a variable load was investigated. The largest oscillations are observed for lower EIS frequencies which resulted in higher energy exchange. The lowest energy exchange which had occurred under higher EIS frequency was addressed and observed through simulation results.

The optimal conversion ratio for SCC in relation to the number of series-connected supercapacitors was explained and analyzed. The TDPR of the SCC was evaluated as an index for specifying the size of the SCC. A trade-off was made between the number of series-connected supercapacitors on the low side of the SCC and the conversion ratio of the SCC.

The allowable window for the voltage level of the supercapacitor string was proposed and considered to avoid exceeding the rated voltage of each individual cell, considering the pre-charged voltage for the supercapacitor string.

Probable limitations were investigated correlating between the switching frequency of the SCCM and the generated EIS perturbation signals, considering the EIS frequency.

In the end, simulation results were presented showing a full functionality of the SCCM as an instantaneous energy buffer.

5.2. Future Work

The proposed SCCM is tailored for NEXA 1.2kW fuel cell stack. Design of the SCCM for other FC stacks with different power ratings can be investigated. Alteration to the conversion ratio of the SCC and the number of series-connected supercapacitors can be determined through the analysis provided in Chapter 3.

Despite the historical belief that SCC are not suitable for high power rating applications, the possibility of interleaving a several SCCMs for FC stacks with higher power rating can be studied. In the attempt for developing interleaved stacked SCCM, the control algorithm implementation for synchronizing the SCCMs can be studied and applied. The possibility of using a combination of film capacitors for higher capacitance and ceramic capacitors for lower capacitance and lower voltage level can be investigated.

Hardware implementation of the SCCM and full set up on an actual FC are listed here for future work. The challenges of this work are listed in Chapter 3 and Chapter 4.

Challenges such as finding the capacitance of each ceramic capacitor bank with respect to their voltage-dependent coefficient need to be addressed.

Bibliography

[1] M. J. Vasallo, J. M. Andújar, C. García, and J. J. Brey, “A Methodology for Sizing Backup Fuel-Cell / Battery Hybrid Power Systems,” vol. 57, no. 6, pp. 1964–1975, 2010.

[2] X. Li, J. Li, L. Xu, F. Yang, J. Hua, and M. Ouyang, “Performance analysis of proton-exchange membrane fuel cell stacks used in Beijing urban-route buses trial project,” *Int. J. Hydrogen Energy*, vol. 35, no. 8, pp. 3841–3847, 2010, doi: 10.1016/j.ijhydene.2010.01.097.

[3] J. S. Lai and M. W. Ellis, “Fuel Cell Power Systems and Applications,” *Proc. IEEE*, vol. 105, no. 11, pp. 2166–2189, 2017, doi: 10.1109/JPROC.2017.2723561.

[4] J. Wu *et al.*, “A review of PEM fuel cell durability: Degradation mechanisms and mitigation strategies,” *J. Power Sources*, vol. 184, no. 1, pp. 104–119, 2008, doi: 10.1016/j.jpowsour.2008.06.006.

[5] H. B. Jensen, E. Schaltz, and P. S. Koustrup, “Evaluation of Fuel-Cell Range Extender Impact on Hybrid Electrical Vehicle Performance,” vol. 62, no. 1, pp. 50–60, 2013.

[6] S. Wang and S. P. Jiang, “Prospects of fuel cell technologies,” *Natl Sci*, pp. 2:163-6, doi: 10.1093/nsr/nwx032.

[7] W. Schmittinger and A. Vahidi, “A review of the main parameters influencing long-term performance and durability of PEM fuel cells,” *J. Power Sources*, vol. 180, no. 1, pp. 1–14, 2008, doi: 10.1016/j.jpowsour.2008.01.070.

[8] L. Dubau *et al.*, “A review of PEM fuel cell durability : materials degradation , local heterogeneities of aging and possible mitigation strategies,” vol. 3, no. December, 2014, doi: 10.1002/wene.113.

[9] L. Carrette and K. A. Friedrich, “Fuel Cells : Principles , Types , Fuels , and Applications **,” pp. 162–193, 2000.

[10] R. Onanena, L. Oukhellou, D. Candusso, F. Harel, D. Hissel, and P. Aknin, “Fuel cells static and dynamic characterizations as tools for the estimation of their ageing time,” *Int. J. Hydrogen Energy*, vol. 36, no. 2, pp. 1730–1739, 2011, doi: 10.1016/j.ijhydene.2010.10.064.

[11] S. Thomas, S. C. Lee, A. K. Sahu, and S. Park, “Online health monitoring of a fuel cell using total harmonic distortion analysis,” *Int. J. Hydrogen Energy*, vol. 39, no. 9, pp. 4558–4565, 2014, doi: 10.1016/j.ijhydene.2013.12.180.

[12] A. Debenjak, J. Petrovčič, P. Boškoski, B. Musizza, and D. Juričić, “Fuel Cell Condition Monitoring System Based on Interconnected DC-DC Converter and Voltage Monitor,” *IEEE Trans. Ind. Electron.*, vol. 62, no. 8, pp. 5293–5305, 2015, doi: 10.1109/TIE.2015.2434792.

[13] J. Shen, H. Homayouni, and J. Wang, “An Online Impedance Processing Method for Fuel Cell EIS Measurements Enabling Degradation Information Extraction,” *IEEE Int. Symp. Ind. Electron.*, vol. 2019-June, pp. 1911–1916, 2019, doi: 10.1109/ISIE.2019.8781344.

[14] X. Yuan, H. Wang, J. Colin Sun, and J. Zhang, “AC impedance technique in PEM fuel cell diagnosis-A review,” *Int. J. Hydrogen Energy*, vol. 32, no. 17, pp. 4365–4380, 2007, doi: 10.1016/j.ijhydene.2007.05.036.

[15] P. Hong, J. Li, L. Xu, M. Ouyang, and C. Fang, “Modeling and simulation of parallel DC/DC converters for online AC impedance estimation of PEM fuel cell stack,” *Int. J. Hydrogen Energy*, vol. 41, no. 4, pp. 3004–3014, 2016, doi: 10.1016/j.ijhydene.2015.11.129.

[16] G. Dotelli, R. Ferrero, P. G. Stampino, S. Latorrata, and S. Toscani, “PEM Fuel Cell Drying and Flooding Diagnosis With Signals Injected by a Power Converter,” *IEEE Trans. Instrum. Meas.*, vol. 64, no. 8, pp. 2064–2071, 2015, doi:

10.1109/TIM.2015.2406051.

[17] M. Marracci, B. Tellini, M. Catelani, and L. Ciani, “Ultracapacitor Degradation State Diagnosis via Electrochemical Impedance Spectroscopy,” vol. 64, no. 7, pp. 1916–1921, 2015.

[18] H. Yang, “A Revisit to Supercapacitor Capacitance Measurement Method 1A of IEC 62391-1,” *2018 IEEE Energy Convers. Congr. Expo. ECCE 2018*, no. 1, pp. 2478–2482, 2018, doi: 10.1109/ECCE.2018.8557429.

[19] H. Homayouni, J. Devaal, F. Golnaraghi, and J. Wang, “Voltage reduction technique for use with electrochemical impedance spectroscopy in high-voltage fuel cell and battery systems,” *IEEE Trans. Transp. Electrif.*, vol. 4, no. 2, pp. 418–431, 2018, doi: 10.1109/TTE.2018.2806090.

[20] J. Shen, H. Homayouni, and J. Wang, “Converter-based Electrochemical Impedance Spectroscopy for High-Power Fuel Cell Stacks with Resonant Controllers,” *IEEE Trans. Ind. Electron.*, vol. 0046, no. c, pp. 1–1, 2020, doi: 10.1109/tie.2020.3016250.

[21] P. Hong, L. Xu, H. Jiang, J. Li, and M. Ouyang, “A new approach to online AC impedance measurement at high frequency of PEM fuel cell stack,” *Int. J. Hydrogen Energy*, vol. 42, no. 30, pp. 19156–19169, 2017, doi: 10.1016/j.ijhydene.2017.06.035.

[22] P. Kreczanik, P. Venet, A. Hijazi, G. Clerc, S. Member, and A. T. B. Presentation, “Study of Supercapacitor Aging and Lifetime Estimation According to Voltage , Temperature , and RMS Current,” *Trans. Ind. Power Electron.*, vol. 61, no. 9, pp. 4895–4902, 2014.

[23] A. S. Weddell, G. V Merrett, T. J. Kazmierski, S. Member, and B. M. Al-hashimi, “Accurate Supercapacitor Modeling for Energy Harvesting Wireless Sensor Nodes,” *Trans. Circuit Syst.*, vol. 58, no. 12, pp. 911–915, 2011.

[24] A. Gebregergis, P. Pillay, and R. Rengaswamy, “PEMFC fault diagnosis,

modeling, and mitigation," *IEEE Trans. Ind. Appl.*, vol. 46, no. 1, pp. 295–303, 2010, doi: 10.1109/TIA.2009.2036677.

[25] K. K. Afridi, M. Chen, S. Member, and D. J. Perreault, "Enhanced Bipolar Stacked SwitchedCapacitor Energy Buffers," *IEEE Trans. Ind. Appl.*, vol. 50, no. 2, pp. 1141–1149, 2014, doi: 10.1109/TIA.2013.2274633.

[26] J. Leuchter, P. Bauer, P. Bojda, and V. Rerucha, "Bi-directional dc- dc converters for supercapacitor based energy buffer for electrical gen-sets," *2007 Eur. Conf. Power Electron. Appl. EPE*, 2007, doi: 10.1109/EPE.2007.4417437.

[27] J. A. Starzyk, Y. W. Jan, and F. Qiu, "A DC-DC charge pump design based on voltage doublers," *IEEE Trans. Circuits Syst. I Fundam. Theory Appl.*, vol. 48, no. 3, pp. 350–359, 2001, doi: 10.1109/81.915390.

[28] S. Xiong and S. Tan, "Cascaded High-Voltage-Gain Bidirectional Switched-Capacitor DC – DC Converters for Distributed Energy Resources Applications," *IEEE Trans. Power Electron.*, vol. 32, no. 2, pp. 1220–1231, 2017.

[29] D. Shin and Y. Kim, "Battery-Supercapacitor Hybrid System for High-Rate Pulsed Load Applications."

[30] S. R. Sanders, E. Alon, H. P. Le, M. D. Seeman, M. John, and V. W. Ng, "The road to fully integrated DC-DC conversion via the switched-capacitor approach," *IEEE Trans. Power Electron.*, vol. 28, no. 9, pp. 4146–4155, 2013, doi: 10.1109/TPEL.2012.2235084.

[31] M. Yassine and D. Fabris, "Performance of commercially available supercapacitors," *Energies*, vol. 10, no. 9, 2017, doi: 10.3390/en10091340.

[32] W. Li, X. Xiang, C. Li, W. Li, and X. He, "Interleaved high step-up ZVT converter with built-in transformer voltage doubler cell for distributed PV generation system," *IEEE Trans. Power Electron.*, vol. 28, no. 1, pp. 300–313, 2013, doi: 10.1109/TPEL.2012.2199771.

[33] A. Khaligh and Z. Li, “Battery, ultracapacitor, fuel cell, and hybrid energy storage systems for electric, hybrid electric, fuel cell, and plug-in hybrid electric vehicles: State of the art,” *IEEE Trans. Veh. Technol.*, vol. 59, no. 6, pp. 2806–2814, 2010, doi: 10.1109/TVT.2010.2047877.

[34] M. Forouzesh, Y. P. Siwakoti, S. A. Gorji, F. Blaabjerg, and B. Lehman, “Step-Up DC-DC converters: A comprehensive review of voltage-boosting techniques, topologies, and applications,” *IEEE Trans. Power Electron.*, vol. 32, no. 12, pp. 9143–9178, 2017, doi: 10.1109/TPEL.2017.2652318.

[35] F. Evran and M. T. Aydemir, “Isolated High Step-Up DC–DC Converter With Low Voltage Stress,” *IEEE Trans. Power Electron. Electron.*, vol. 29, no. 7, pp. 3591–3603, 2014.

[36] Y. Lo and J. Lin, “Active-Clamping ZVS Flyback Converter Employing Two Transformers,” vol. 22, no. 6, pp. 2416–2423, 2007.

[37] J. M. Henry and J. W. Kimball, “Practical performance analysis of complex switched-capacitor converters,” *IEEE Trans. Power Electron.*, vol. 26, no. 1, pp. 127–136, 2011, doi: 10.1109/TPEL.2010.2052634.

[38] H. Saif *et al.*, “A wide load current and voltage range switched capacitor DC–DC converter with load dependent configurability for dynamic voltage implementation in miniature sensors,” *Energies*, vol. 11, no. 11, pp. 1–21, 2018, doi: 10.3390/en11113092.

[39] Y. Ni, S. Pervaiz, S. Member, M. Chen, and K. K. Afridi, “Energy Density Enhancement of Stacked Switched Capacitor Energy Buffers Through Capacitance Ratio Optimization,” *IEEE Trans. Power Electron.*, vol. 32, no. 8, pp. 6363–6380, 2017.

[40] Y. Zhang, Y. Gao, J. Li, and M. Sumner, “Interleaved switched-capacitor bidirectional DC-DC converter with wide voltage-gain range for energy storage systems,” *IEEE Trans. Power Electron.*, vol. 33, no. 5, pp. 3852–3869, 2018, doi:

10.1109/TPEL.2017.2719402.

[41] E. M. Ali, N. Z. Yahaya, P. Nallagownden, and B. H. Alqasem, “Enhanced Dickson voltage multiplier rectenna by developing analytical model for radio frequency harvesting applications,” *Int. J. RF Microw. Comput. Eng.*, vol. 29, no. 1, pp. 1–10, 2019, doi: 10.1002/mmce.21657.

[42] A. Kushnerov, S. Member, S. Ben-yaakov, and P. O. Box, “Algebraic Synthesis of Fibonacci Switched Capacitor Converters,” pp. 18–21.

[43] P. Junior, S. Costa, C. Henrique, and I. Font, “Single-Phase Hybrid Switched-Capacitor,” vol. 33, no. 6, pp. 5118–5130, 2018.

[44] M. Liu, “Demystifying Switched Capacitor Circuits.” Newnes, p. 317p, 2006.

[45] W. Li and X. He, “Review of nonisolated high-step-up DC/DC converters in photovoltaic grid-connected applications,” *IEEE Trans. Ind. Electron.*, vol. 58, no. 4, pp. 1239–1250, 2011, doi: 10.1109/TIE.2010.2049715.

[46] A. Cervera, M. Evzelman, M. M. Peretz, and S. S. Ben-Yaakov, “A high-efficiency resonant switched capacitor converter with continuous conversion ratio,” *IEEE Trans. Power Electron.*, vol. 30, no. 3, pp. 1373–1382, 2015, doi: 10.1109/TPEL.2014.2317758.

[47] Y. Lei, Z. Ye, and R. C. N. Pilawa-Podgurski, “A GaN-based 97% efficient hybrid switched-capacitor converter with lossless regulation capability,” *2015 IEEE Energy Convers. Congr. Expo. ECCE 2015*, pp. 4264–4270, 2015, doi: 10.1109/ECCE.2015.7310262.

[48] Y. Zhang, Q. Liu, Y. Gao, J. Li, M. Sumner, and S. Member, “Hybrid Switched-Capacitor / Switched-Quasi- Z-Source Bidirectional DC – DC Converter With a Wide Voltage Gain Range for Hybrid Energy Sources EVs,” vol. 66, no. 4, pp. 2680–2690, 2019.

[49] S. Li, K. Xiangli, and Y. Zheng, “Analysis and Design of the Ladder Resonant

Switched-Capacitor Converters for Regulated," vol. 64, no. 10, pp. 7769–7779, 2017.

[50] H. P. Le, S. R. Sanders, and E. Alon, "Design techniques for fully integrated switched-capacitor DC-DC converters," *IEEE J. Solid-State Circuits*, vol. 46, no. 9, pp. 2120–2131, 2011, doi: 10.1109/JSSC.2011.2159054.

[51] M. S. M. and D. Maksimovic, "Performance limits of switched-capacitor DC-DC converters," *Proc. PESC '95 - Power Electron. Spec. Conf. Atlanta, GA, USA*, vol. 2, pp. 1215–1221, 1995, doi: 10.1109/PESC.1995.474969.

[52] Y. Ye, K. W. E. Cheng, J. Liu, and K. Ding, "A step-up switched-capacitor multilevel inverter with self-voltage balancing," *IEEE Trans. Ind. Electron.*, vol. 61, no. 12, pp. 6672–6680, 2014, doi: 10.1109/TIE.2014.2314052.

[53] Y. Jiang, M. K. Law, Z. Chen, P. I. Mak, and R. P. Martins, "Algebraic Series-Parallel-Based Switched-Capacitor DC-DC Boost Converter with Wide Input Voltage Range and Enhanced Power Density," *IEEE J. Solid-State Circuits*, vol. 54, no. 11, pp. 3118–3134, 2019, doi: 10.1109/JSSC.2019.2935556.

[54] R. Barzegarkhoo, E. Zamiri, N. Vosoughi, H. M. Kojabadi, and L. Chang, "Cascaded multilevel inverter using series connection of novel capacitor-based units with minimum switch count," *IET Power Electron.*, vol. 9, no. 10, pp. 2060–2075, 2016, doi: 10.1049/iet-pel.2015.0956.

[55] Y. Wu, Y. Mustafa, and Y. Lu, "A Switched-Capacitor DC-DC Converter with Unequal Duty Cycle for Ripple Reduction and Efficiency Improvement," no. 201807010065, pp. 2019–2020, 2019.

[56] A. Ballo, A. D. Grasso, and G. Palumbo, "A review of charge pump topologies for the power management of IoT nodes," *Electron.*, vol. 8, no. 5, 2019, doi: 10.3390/electronics8050480.

[57] A. Eltaliawy, H. Mostafa, and Y. Ismail, "Circuit design techniques for increasing the output power of switched capacitor charge pumps," *Can. Conf. Electr. Comput.*

Eng., pp. 1–5, 2014, doi: 10.1109/CCECE.2014.6900953.

[58] H. Yang, "Estimation of Supercapacitor Charge Capacity Bounds Considering Charge Redistribution," *IEEE Trans. Power Electron.*, vol. 33, no. 8, pp. 6980–6993, 2018, doi: 10.1109/TPEL.2017.2764423.

[59] Y. Perrin, A. Galisultanov, H. Fanet, and G. Pillonnet, "Optimal Charging of Nonlinear Capacitors," vol. 34, no. 6, pp. 5023–5026, 2019.